MINISTÉRIO DA EDUCAÇÃO

UNIVERSIDADE FEDERAL DO RIO GRANDE DO NORTE - UFRN

CENTRO DE CIÊNCIAS DA SAÚDE - CCS

PROGRAMA DE PÓS-GRADUAÇÃO EM CIÊNCIAS DA SAÚDE - PPGCSA

NANOPARTÍCULAS DE OURO ESFÉRICAS NEUTRAS ATUAM NA RESPOSTA ANTI-INFLAMATÓRIA, ANTIOXIDANTE E ANTIFIBROTICA EM LESÃO HEPÁTICA INDUZIDA POR ÁLCOOL E METANFETAMINA EM RATOS WISTAR

THAIS GOMES DE CARVALHO

NATAL / RN

2018

THAIS GOMES DE CARVALHO

NANOPARTÍCULAS DE OURO ESFÉRICAS NEUTRAS ATUAM NA RESPOSTA ANTI-INFLAMATÓRIA, ANTIOXIDANTE E ANTIFIBRÓTICA EM LESÃO HEPÁTICA INDUZIDA POR ÁLCOOL E METANFETAMINA EM RATOS WISTAR

Dissertação apresentada ao Programa de Pós-Graduação em Ciências da Saúde da Universidade Federal do Rio Grande do Norte - UFRN como requisito obrigatório para a obtenção do título de Mestre em Ciências da Saúde.

Orientador: Prof. Dr. Raimundo Fernandes de Araújo Junior

NATAL / RN

2018

III

MINISTÉRIO DA EDUCAÇÃO

UNIVERSIDADE FEDERAL DO RIO GRANDE DO NORTE

CENTRO DE CIÊNCIAS DA SAÚDE

PROGRAMA DE PÓS-GRADUAÇÃO EM CIÊNCIAS DA SAÚDE

Coordenadora do Programa de Pós-graduação em Ciências da Saúde
Profª Drª Ana Katherine da Silveira Gonçalves de Oliveira

Universidade Federal do Rio Grande do Norte - UFRN
Sistema de Bibliotecas - SISBI
Catalogação de Publicação na Fonte. UFRN - Biblioteca Setorial do Centro Ciências da Saúde - CCS

Carvalho, Thaís Gomes de.
Nanopartículas de ouro esféricas neutras atuam na resposta anti-inflamatória, antioxidante e antifibrotica em lesão hepática induzida por álcool e metanfetamina em ratos wistar / Thaís Gomes de Carvalho. - 2018.
86f.: il.

Dissertação (Mestrado em Ciências da Saúde) - Universidade Federal do Rio Grande do Norte, Centro de Ciências da Saúde, Programa de Pós-Graduação em Ciências da Saúde. Natal, RN, 2018.
Orientador: Prof. Dr. Raimundo Fernandes de Araújo Junior.

1. Nanopartículas de ouro - Dissertação. 2. Álcool - Dissertação. 3. Metanfetamina - Dissertação. 4. Hepatotoxicidade - Dissertação. 5. Células de Kupffer - Dissertação. I. Araújo Junior, Raimundo Fernandes de. II. Título.

RN/UF/BSCCS CDU 615.015.14:616.36

Elaborado por Adriana Alves da Silva Alves Dias - CRB-15/474

THAIS GOMES DE CARVALHO

NANOPARTÍCULAS DE OURO ESFÉRICAS NEUTRAS ATUAM NA RESPOSTA ANTI-INFLAMATÓRIA, ANTIOXIDANTE E ANTIFIBRÓTICA EM LESÃO HEPÁTICA INDUZIDA POR ÁLCOOL E METANFETAMINA EM RATOS WISTAR

Aprovada em 03 / 08 / 2018

- Comissão Examinadora

Nome	Função	Assinatura
Raimundo Fernandes de Araújo Junior	Presidente – UFRN	
Caroline Addison Carvalho Xavier de Medeiros	Membro Titular – UFRN	
Leônia Maria Batista	Membro Externo – UFPB	

DEDICATÓRIA

Dedico esse trabalho a minha família ao meu pai por não medir esforços para realização dos meus sonhos e por me apoiar em todos os momentos, e a toda minha família pelo incentivo que recebi durante toda a minha vida para ver os estudos com bons olhos e com a esperança de que um dia todo esse esforço valeria a pena, e eles estavam certos, vale a pena, muito obrigada por não desistir de mim.

Essa vitória vai para vocês família aos que acreditaram e a também os descrentes eu consegui, dedico também a minha mãe aquela que a 23 anos atrás teve que abrir mão de ver sua filha crescer e deixá-la com uma boa família para que ela tivesse um bom futuro, então querida mãe estou vivendo da melhor forma que posso, e desfrutando da oportunidade que você gostaria que eu tivesse há e à minha madrinha também que ocupou por vezes o papel de mãe na minha vida e disse que nós temos a obrigação de fazer coisas boas em nossas vidas, espero que essa seja uma coisa boa.

AGRADECIMENTOS

Durante esses dois anos só tenho a agradecer a todos que passaram pelo meu caminho e que com certeza deixaram um pouco de si. Os momentos de alegria com meus amigos e colegas de trabalho em laboratório que me permitiram acreditar na beleza da vida, e me consolaram nos momentos de sofrimento. As somas de todos os acontecimentos vividos durante o mestrado contribuíram para me tornar a pessoa que sou hoje. É muito difícil transformar sentimentos em palavras, mas serei eternamente grata a vocês, pessoas imprescindíveis para a realização e conclusão deste trabalho.

Primeiramente, agradeço ao meu orientador Raimundo Fernandes de Araújo Junior, por acreditar que eu era capaz e pela orientação. Mesmo chegando sem me conhecer direito, você abriu as portas, como um pai que abre os braços para receber um filho. Nesse mundo, repleto de pessoas ruins, você me faz acreditar que os bons são a maioria. Só tenho a agradecer aos seus ensinamentos (pessoais e acadêmicos), orientações, palavras de incentivo, puxões de orelha, paciência e dedicação.

A professora Aurigena Antunes pelos ensinamentos, orientações, incentivo, amizade e dedicação. Você esteve ao meu lado desde os primeiros experimentos e mudou a visão que eu tinha de orientação, e não mediu esforços para me ajudar, sempre com uma solução simples para os meus problemas que pareciam ser gigantes.

Aos animais, parte fundamental desse trabalho, obrigada por suas contribuições à ciência.

À seção de pós-graduação de Ciências da Saúde – UFRN e ao Profº. Drº Sócrates Egito, pela atenção, apoio e profissionalismo.

Ao CNPq pelo auxílio e apoio financeiro concedido, que foi de fundamental importância para o desenvolvimento deste trabalho.

Por fim, a todos aqueles que contribuíram, direta ou indiretamente, para a realização desta dissertação, o meu sincero agradecimento.

“De tudo, ficaram três coisas: a certeza de que ele estava sempre começando, a certeza de que era preciso continuar e a certeza de que seria interrompido antes de terminar. Fazer da interrupção um caminho novo. Fazer da queda um passo de dança, do medo uma escada, do sono uma ponte, da procura um encontro.

Fernando Sabino Sabino

RESUMO

Este estudo teve como objetivo elucidar os efeitos terapêuticos das nanopartículas de ouro esféricas neutras em ratos com lesão hepática induzida por álcool e metanfetamina (METH). A lesão hepática foi induzida por administrações via gavagem oral de solução alcoólica 30% (7 mg/kg) uma vez por dia durante 28 dias, seguido de METH (10 mg/kg) nos 20º e 28º dias de tratamento. Para avaliar o efeito terapêutico, três doses de GNPs foram testadas: 724,96 µg/kg, 362,48 µg/kg e 181,48 µg/kg. Após a realização de testes de Biodistribuição as GNPs migraram para fígado, baço, bexiga, rins e cérebro. As GNPs foram absorvidas pelas células de Kupffer no fígado, conforme observado na análise tecidual. O tratamento com GNPs (724,96 µg/kg) durante o protocolo de exposição ao álcool e METH foi associado a redução da esteatose, degeneração do cordão hepático, fibrose e necrose, bem como redução dos níveis de AST, ALT, TG, MPO, MDA, GSH e citocinas pró-inflamatórias IL-1β e TNF-α e níveis aumentados de citocinas regulatórias como a IL-10, quando comparadas com o grupo controle positivo álcool + METH. O tratamento com 724,96 µg/kg de GNPs também reduziu os níveis de expressão de TGF-β, FGF-1, SOD-1 e GPx-1 e diminuiu a expressão de citocinas pró-inflamatórias como IL-1β, TNF-α e MIF. Houve uma diminuição na expressão de RNAm de pró-colágeno tipo I e III (PCI, PCIII), fator nuclear kappa B (NF-Kβ), a adesão específica de macrófagos (F4/80), proteína cinase B (AKT) e fosfatidilinositol-4, 5-bisphosphate 3-cinase (PI3K) no grupo tratado com álcool + METH + 724,96 µg/kg de GNPs em relação ao grupo controle positivo tratado com álcool + METH. As GNPs reduziram a atividade de células de Kupffer e células estreladas hepáticas que afetaram o perfil de estimulação de citocinas pró-inflamatórias, redução do estresse oxidativo e consequentemente o desenvolvimento de fibrose hepática por meio da modulação das vias de sinalização da AKT/ PI3K/ERK.

Palavras-chave: nanoparticulas de ouro, álcool, metanfetamina, hepatotoxicidade e células de Kupffer.

ABSTRACT

This study aimed to elucidate the therapeutic effects of gold nanoparticles (GNPs) in rats with alcohol and methamphetamine-induced hepatic injury (METH). Hepatic injury was induced by administrations via gavage of 30% alcoholic solution (7 mg/kg) once daily for 28 days, followed by METH (10 mg/kg) on the 20th and 28th days of treatment. To evaluate the dose-dependent effect, doses of GNPs were fractionated at 724.96 µg/kg, 362.48 µg/kg and 181.48 µg/kg. After conducting Biodistribution tests the GNPs migrated to the liver, spleen, bladder, kidneys and brain. The GNPs were absorbed by the Kupffer cells in the liver, as observed in the tissue analysis. Treatment with GNPs (724.96 µg/kg) during the alcohol and METH protocol was associated with reduced steatosis, hepatic cord degeneration, fibrosis and necrosis, as well as reduced levels of AST, ALT, TG, MPO , MDA, GSH and proinflammatory cytokines IL-1β and TNF-α and increased levels of regulatory cytokines such as IL-10, when compared with the positive alcohol + METH control group. Treatment with 724.96 µg / kg of GNPs also reduced expression levels of TGF-β, FGF-1, SOD-1 and GPx-1 and decreased expression of proinflammatory cytokines such as IL-1β, TNF-α and MIF. There was a decrease in the expression of procollagen type I and III mRNA (PCI, PCIII), nuclear factor kappa B (NF-Kβ), macrophage specific adhesion (F4/80), protein kinase B (AKT) and phosphatidylinositol -4,5-bisphosphate 3-kinase (PI3K) in the alcohol treated group + METH + 724.96 µg / kg of GNPs in relation to the positive control group treated with alcohol + METH. GNPs reduced the activity of Kupffer cells and hepatic stellate cells that affected the proinflammatory cytokine stimulation profile, reduction of oxidative stress and consequently the development of hepatic fibrosis by modulating AKT / PI3K / ERK signaling pathways.

Keywords: Gold nanoparticles, ethanol, methamphetamine, toxicity and Kupffer cells.

LISTA DE ABREVIATURAS E SIGLAS

AST – Aspartato aminotrasferase

ALT – Alanina aminotransferase

TG – Triglicerídeos

GNPs – Nanopartículas de ouro

METH - Metanfetamina

MPO - Mieloperoxidase

MDA - Malonaldeído

GSH – Glutationa reduzida

GPX-1 – Glutationa peroxidase

PI3K - fosfatidilinositol - 4, 5-bisfosfato 3-cinase

AKT– Serina / Treonina kinase

ERK/1/2 - Cinase regulada por sinal extracelular

NF-KB - Fator nuclear kappa B

TNF-α - Fator de necrose tumoral alfa

MIF – Fator inibidor da migração de macrófago

TGF-B – Fator de crescimento transformador

FGF – Fator de crescimento fibroblástico

IL-1B – Interleucina 1 beta

IL-10 – Interleucina 10

HSC – Células estreladas hepáticas

TCA – Ácido tricloroacético

HCl - Ácido clorídrico

FCK - Ferrocianeto de potássio

LISTA DE FIGURAS

LISTA DE TABELA

Tabela 1 – Sequência de primers analisados no RT - PCR

SUMÁRIO

1 – INTRODUÇÃO

O consumo de drogas é universal nas diferentes culturas humanas em todos os tempos[1]. O homem pela sua própria natureza procura alternativas para aumentar a sensação de prazer e diminuir o desconforto e o sofrimento. Para tanto, utiliza de maneira indiscriminada substâncias capazes de modificar o funcionamento do sistema nervoso, induzindo sensações corporais e estados psicológicos alterados[2]. Entre as substâncias que são coadministradas com drogas ilícitas, o etanol é, sem dúvida, o químico mais prevalente responsável pelo aumento do número de internações e mortes hospitalares[1].

Segundo relatório da Organização mundial de Saúde de 2014, a probabilidade que o indivíduo tem de desenvolver cirrose é de 30% tendo o álcool como um fator que desencadeia a progressão da doença[2]. Transtornos relacionados ao uso de anfetaminas representam uma parte considerável da carga global de doenças atribuíveis a transtornos por uso de drogas, somente àquelas relacionadas ao uso de opióides. Dados acessíveis mostram que, entre as anfetaminas, a metanfetamina representa a maior ameaça à saúde global.

O etanol é frequentemente co-utilizado com drogas psico-estimulante, como metanfetamina ou cocaína[3], a fim de aumentar e prolongar os efeitos das drogas. Além disso, o etanol pode alterar a expressão e/ou a atividade de algumas enzimas que metabolizam drogas[4], incluindo aqueles que estão envolvidos no metabolismo da METH. Além disso, os usuários de METH são consumidores regulares de álcool antes de seu primeiro contato com METH[5], o que pode representar um fator de risco para a interação tóxica entre estas duas drogas[6]. Evidências sugerem que a coadministração de etanol e as anfetaminas produzem um efeito subjetivo amplificado e estendido[7], mas poucos estudos examinaram o impacto somático da combinação metano-etanol no cérebro[8–10].

A doença hepática alcoólica (DHA) é a lesão do fígado que diz respeito a uma variedade de alterações hepáticas que surgem após anos de consumo excessivo de álcool[11]. Trata-se de uma doença multifatorial, complexa e representa um espectro de doenças e alterações morfológicas que variam

desde a esteatose, à inflamação e necrose hepática (hepatite alcoólica) à fibrose progressiva e cirrose. Além disso, o consumo excessivo de álcool favorece a progressão de outras patologias hepáticas, tais como as hepatites virais C e B e o carcinoma hepatocelular (CHC)[12].

Três mecanismos foram propostos para desenvolvimento da lesão hepática alcoólica: (I) toxicidade do acetaldeído[13]; (II) geração metabólica de espécies reativas de oxigênio (ROS) ou exposição ao estresse oxidativo[14,15]; e (III) estresse oxidativo em hepatócitos causado por resposta imune[16,17]. Assim, o estresse oxidativo é sem dúvida uma força motriz na doença hepática alcoólica, pois dá início à peroxidação lipídica que danifica diretamente o plasma e as membranas intracelulares e induz a produção de grupos aldeídos reativos com potentes propriedades pró-inflamatórias e pró-fibróticas[18].

Estudos recentes indicaram que a etiopatogenia da DHA está profundamente ligada não só com o metabolismo do etanol mas também com o stress oxidativo, a depleção de glutationa, indução mediada pelo etanol da libertação de endotoxinas do intestino e consequente ativação das células de Kupffer e as células estreladas hepáticas[19].

A doença hepática alcoólica engloba vários estágios, assim o seu espectro é diverso e inclui: a esteatose hepática alcoólica, hepatite alcoólica, fibrose alcoólica, cirrose alcoólica e hepatocarcionoma. Estes estágios não são necessariamente fases distintas da evolução da doença, mas sim, várias etapas que podem estar presentes simultaneamente num dado indivíduo, sob a influência de inúmeros fatores de risco[11].

A esteatose é a manifestação mais precoce, mais frequente e menos grave da doença alcoólica hepática, que compromete o parênquima hepático e caracteriza-se pela acumulação de gordura nos hepatócitos, decorrente do consumo crónico do etanol[20-21].

A hepatite alcoólica é um processo inflamatório associado à necrose hepatocitária, resultante do consumo excessivo de álcool e considerada como uma lesão pré-cirrótica. Desta forma, a hepatite alcoólica é caracterizada pela infiltração do fígado por células inflamatórias e lesões hepatocelulares, podendo-se desenvolver em pacientes com esteatose e sendo associada à fibrose progressiva[22].

A fibrose hepática alcoólica pode ser definida como uma resposta de cicatrização às lesões hepáticas desencadeadas pelo abuso crônico de etanol e é caracterizada por uma deposição excessiva de matriz extracelular, que inclui três grandes famílias de proteínas: glicoproteínas colágeno e proteoglicanos[23].

O etanol promove a fibrinogênese tanto através do seu metabólito primário, o acetaldeído, assim como pelo desenvolvimento de ROS, que ao originar estresse oxidativo ativa as células de Kupffer, aumentando a produção de citocinas pró-inflamatórias e consequente ocorre a ativação das células estreladas hepáticas. Nesta sequência, as células hepáticas estreladas, localizadas no espaço de Disse, e quando ativadas, proliferam-se e adquirem as características de miofibroblastos[23-24]. Neste contexto, a deposição excessiva da matriz extracelular é resultante do desequilíbrio entre a fibrinogênese e a fibrose no fígado, sendo que a deposição de matriz extracelular passa a ser maior que a sua remoção, principalmente a nível de colágeno tipo I e II, mas também proteoglicanos e glicoproteínas[25].

Na lesão hepática, as células de Kupffer ativadas liberam vários agentes solúveis, incluindo citocinas, como TGF-β e TNF-α[26] e o fator nuclear kappa B (NF-κB) transloca-se para o núcleo, na qual se liga ao promotor de genes alvo, como o TNF-α e outras citocinas pró-inflamatórias[27]. Esses fatores atuam nas células estreladas hepáticas (HSC), localizadas no espaço parassinusoidal[28]. A fosfatidil-inositol - 4, 5 - bisfosfato 3 - cinase ativada (PI3-K) participa na regulação da migração, proliferação, secreção e adesão de colágeno de HSC além de estar envolvida na regulação de várias respostas celulares, como o crescimento celular, sobrevivência e migração. A proteína quinase B (AKT ou PKB) está a jusante de PI3-K e a ativação de AKT está associada à proliferação de HSC e à transcrição e tradução de colágeno α1 (I)[29].

Nanopartículas esféricas de ouro funcionalizadas (GNPs) com propriedades geométricas e ópticas controladas são objeto de estudos intensivos e aplicações biomédicas, incluindo genômica, biossensores, imunoensaio químico[30-31], fototerapia a laser de células cancerígenas[32], a entrega direcionada de drogas[33], DNA e antígenos[34], bio-imagem óptica e o monitoramento de células[35] e tecidos com o uso de sistemas de detecção de última geração.

A biossegurança do ouro metálico é bem compreendida e tem sido utilizada *in vivo* desde a década de 1950[36]. A investigação da citotoxicidade dos GNPs concentra-se em seu tamanho, forma, doses e ligantes circunvizinhos, sendo aqueles quimicamente positivos e negativos responsáveis por causar danos às células através de alterações oxidativas no potencial de membrana mitocondrial[37-38]. As GNPs neutras esféricas são mais adequados para aplicação biomédica devido à sua incapacidade de remover elétrons de moléculas, como lipídios de membrana e mitocôndrias, além de não gerar radicais livres[39-40].

Macrófagos locais, como as células de Kupffer, ingerem materiais estranhos, como patógenos e nanopartículas, e recrutam macrófagos adicionais para o microambiente inflamado, produzindo citocinas, incluindo TNF-α, IL-6 e TGF-β, que regulam positivamente o processo inflamatório[41]. As nanopartículas positivamente carregadas são preferencialmente absorvidas por macrófagos derivados de monócitos e células de Kupffer que possuem um fenótipo tipo M2 que produz alto nível de TGF-β[42].

Nesse contexto, macrófagos como as células de Kupffer, portanto, não apenas representam alvos atraentes para a nanomedicina na doença hepática, mas também precisam ser considerados como potenciais eliminadoras de partículas em qualquer tipo de administração parenteral de nanopartículas. Como tal, a alteração do comportamento das células de Kupffer que pode afetar o progresso de distúrbios relacionados à inflamação. Portanto, o objetivo do presente trabalho foi avaliar o efeito anti-inflamatório, antioxidante e anti-fibrótico das GNPs em um modelo animal de lesão hepática induzida por etanol e METH.

2 – OBJETIVOS

2.1 - Objetivo geral

Investigar os efeitos anti-inflamatórios, antifibróticos e antioxidantes das Nanoparticulas de ouro esféricas em fígado de Ratos Wistar com lesão hepática induzida pela associação do álcool e metanfetamina.

2.2 - Objetivos específicos

1 - Analisar a atividade anti-inflamatória das nanoparticulas de ouro através da quantificação de citocinas como IL-1β, TNF-α e IL-10 em fígado de ratos no modelo de injúria hepática.

2. Averiguar os níveis de mieloperoxidase (MPO) e do estresse oxidativo como malonaldeído (MDA) e a glutationa reduzida (GSH) no fígado dos animais submetidos a diferentes doses de GNPs.

3. Avaliar alterações histo-morfológicas provocadas através da exposição dos animais as GNPs, álcool e metanfetamina.

4. Analisar alterações da função hepática através dos marcadores AST, ALT e TG.

5. Analisar o perfil anti-fibrótico, através do estudo da atividade das células estreladas, e a participação da via AKT-PI3K-ERK1/2 no fígado.

6. Observar o perfil de Biodistribuição das GNPs 48hs após a administração a nível sistêmico, em tecido hepático e nas células de Kupffer.

3 – JUSTIFICATIVA

Entender os mecanismos deletérios no fígado causados pelos metabólitos do álcool e da METH, uma combinação cada vez crescente por jovens dos 16 aos 30 anos de idade como drogas recreativas[43], são de fundamental importância para pesquisa de novos fármacos que atenuem ou bloqueiem esses efeitos, visto que a agressão causada pela combinação crônica dessas substâncias químicas leva ao desenvolvimento de esteato-hepatite, uma condição inflamatória grave como falência das atividades funcionais do órgão[44].

A Nanomedicina tem promovido o desenvolvimento de sistemas eficazes para carrear drogas, modificando o perfil farmacocinético do fármaco, assim como, diminuindo os efeitos colaterais dos mesmos[45], sendo as GNPs sistemas promissores para esse fim. Além disso, entender as vias de sinalização que deflagram a inflamação e consequentemente a fibrose em modelo animal tornam este estudo de grande relevância científica, já que abrirá inferências para novos sistemas de associação de droga, visto que ainda não se tem conhecimento do uso das GNPs para o tratamento de Doença Hepática Alcoólica associada à METH.

4 – MATERIAIS E MÉTODOS

4.1 - Produtos Químicos

O álcool etílico absoluto (PA 99,8%) foi obtido da Vetec Química, Brasil. A metanfetamina foi adquirida da Fisher Scientific, de acordo com a lei 10.357 de 27 de dezembro de 2001, que estabelece regras para produção, controle e inspeção de substâncias químicas.

As células de macrófagos de murinos (RAW 264.7; cat. No.TIB-71) foram obtidas na American Type Culture Collection (Manassas, VA, EUA). O meio de Eagle modificado por Dulbecco (DMEM) foi adquirido da Invitrogen Corporation (Carlsbad, CA, EUA); soro bovino fetal da Hyclone Company (Logan, UT, EUA).

Anticorpos anti-TGF-β, FGF, SOD-1, GPX, IL-1-β, TNF-β e MIF foram obtidos de Santa Cruz Biotechnology Enterprise, Brasil o anticorpo secundário conjugado com estreptavidina-HRP (Biocare Medical, Concord, CA, EUA), Kit Trek Avidin-HRP Label + Kit (Biocare Medical, Dako, EUA), IL-1β, IL-10, TNF-α e ELISA (R & D Systems, Minneapolis, MN, USA) também foram utilizados neste estudo.

4.2 - Cultura de células

Células de macrófagos RAW 264.7 foram cultivadas em meio DMEM com 10% de soro bovino fetal. As células foram semeadas a uma densidade de $5x10^4$ células por poço em placas de 6 poços e atingiram 50-60% de confluência 24 h após semeadas, imediatamente antes da exposição à concentração não citotóxica de GNPs em 10 µg/mL para tratamento[46]. As células foram mantidas em incubadora de CO^2 a 5% a 37ºC e com 95% de umidade. As células foram subsequentemente analisadas por um microscópio de contraste de fase.

4.3 - Imuno-Fluorescência – In Vitro

As células de macrófagos RAW 264.7 foram plaqueadas em placas de 24 poços (5 x 10^4 células) e deixadas a crescer durante 24 h. As células foram então lavadas, fixadas com 1% de paraformaldeído, permeabilizadas com

Triton-X e incubadas com 100 µL de GNPs e 4, 6-diamidino-2-fenilindol foi usado para coloração nuclear por 10 minutos em atmosfera úmida à temperatura ambiente. Experimentos de controle foram realizados sob as mesmas condições, mas sem a adição de GNPs. As placas de vidro foram então diretamente observadas com o microscópio de fluorescência - Leica DM5500 B (configurações de filtro: TXR, Cy7, FITC e DAPI), equipado com um condensador usando excitação a laser de 512 a 542 nm.

4.4 - Animais

Ratos Wistar machos, pesando entre 270g - 300g, obtidos do biotério do departamento de farmacologia da Universidade Federal do Rio Grande do Norte, Natal, Brasil, foram utilizados para experimentos. Os animais foram alojados em gaiolas com livre acesso a alimentos e água em ambiente controlado de temperatura e umidade sob um ciclo claro/escuro de 12 horas. Os animais foram tratados de acordo com os princípios éticos para experimentação animal. Todos os experimentos foram aprovados pelo Comitê de Ética da UFRN (número de aprovação: 018/2015).

4.5 - Preparação e administração de etanol

Utilizou-se 7g por kg de peso corporal de solução de etanol a 30% v/v como dose crônica neste modelo animal, 30g de etanol absoluto foram dissolvidos em água destilada e completados até 100 ml e 6,2 ml da solução foram administrados diariamente durante 28 dias a cada rato tratado com etanol[47].

4.6 - Preparação e administração de metanfetamina

Para a metanfetamina utilizou-se a dose de 10 mg/kg, na qual foram diluídos 25 mg de metanfetamina em 10 ml de água destilada. Cada animal recebeu 0,1 ml desta solução, o que corresponde a 2,5 mg em cada dose[48].

4.7 - Produção de nanopartículas de ouro

GNPs foram obtidas em parceria com o Departamento de Química da Universidade Federal do Rio Grande do Norte. Essas GNPs são produzidos conforme descrito por[50].

Primeiro, o Au^{3+} foi reduzido por glicerol em meio alcalino e a polivinilpirrolidona foi usada para estabilizar as nanopartículas de ouro. O HCl diluído foi então adicionado para levar o pH da solução a 7 e gerar GNPs neutras. Considerando a transformação quantitativa de íons de ouro em nanopartículas, a concentração de GNPs foi estimada em 197 $\mu g/mL^{-1}$. A mistura final tem uma cor vermelho-escura devido à formação de GNPs de 7,4 ± 1,6 nm de tamanho.

Utilizou-se um sistema Zeta-Meter 3.0+ (Zeta-Meter Inc., EUA) a uma temperatura de 25 ± 2 °C para determinar a mobilidade eletroforética da solução coloidal de GNPs (20 mL). O potencial zeta foi calculado usando a equação de Smoluchowski:

$$\zeta = \frac{\mu_E \eta_0}{\varepsilon_0 \varepsilon_r},$$

Onde μE é a mobilidade eletroforética, onde η_0 é a viscosidade de fase contínua, ε_0 é a permitividade de um vácuo e r é a permeabilidade relativa da fase contínua.

4.8 - Dosagem e administração de nanopartículas de ouro

As doses de GNPs foram escolhidas através de um projeto piloto, as doses de 700 μg/kg, 1000 μg/kg e 1.500 μg/kg foram testadas. A dose 700 μg/kg apresentou melhores resultados na diminuição das citocinas inflamatórias IL-1β e TNF-α[48]. A dose de 700 μg/kg foi utilizada para calcular as doses a serem utilizadas no experimento, com base em uma formulação de nanopartículas de ouro com concentração de 197 $\mu g/mL^{-1}$.

As doses foram ajustadas para que, para todos os grupos tratados por via oral por sonda esofágica, o volume final utilizado fosse padronizado em 1ml. A fim de avaliar o efeito terapêutico, as doses foram fracionadas em 3: começando com a dose mais alta: 724,96 μg/kg (GNP3); uma dose intermediária correspondente a 362,48 μg/kg (GNP2); a terceira dose: 181,48 μg/kg (GNP1).

4.9 - Indução de etanol e lesão hepática induzida por metanfetamina

O protocolo para indução de lesão hepática desenvolvido através da exposição ao álcool e METH é resumido abaixo.

1). Administração do tratamento 1 hora antes da administração de etanol (30%). Cada tratamento tem três doses a serem testadas (o volume administrado dependerá do peso médio dos animais).

2). Após 1 hora da administração do tratamento, 30% de etanol deve ser administrado. A dose de etanol é de 7 g/kg;

3). Salina (NaCl 0,9%) deve ser administrada uma vez por semana, a cada seis dias, durante a primeira e segunda semana de indução de lesão hepática; isto deve ser administrado após 3 horas de administração da solução de etanol a 30%. Esta solução salina irá simular a metanfetamina usada na 3ª e 4ª semana.

4). Repita os passos 1 e 2 durante 7 dias.

5). Repita o passo 3 uma vez por semana, a cada 7 dias, totalizando 28 dias de indução de lesão hepática.

A eutanásia foi realizada no 29º dia por injeção intraperitoneal de Ketamina 50 mg/mL e Xilazina 20 mg/mL. Todos os grupos de animais foram mantidos em jejum por 12 horas para realizar a análise bioquímica subsequente. Uma vez inconsciente, os animais foram submetidos a punção cardíaca seguida de remoção do fígado.

Fragmentos de fígado foram congelados a -80 °C para análise de citocinas e estresse oxidativo, quantificação de proteínas via Western blot, RT-PCR e biodistribuição. Outros fragmentos de fígado foram imersos em formalina tamponada a 10% para análise histopatológica.

4.10 - Biodistribuição de nanopartículas de ouro

Conjugação de fluorescência do infravermelho próximo (NIR) para os GNPs

As GNPs foram conjugadas com o grupo tiol do cloridrato de poli (etilenoglicol) alfa-amino-omega-mercapto (SH-PEG-NH2, PM 3.000 g/mol) durante 3 h à temperatura ambiente. O excesso de SH-PEG-NH^2 não conjugado foi removido por diálise (durante três dias numa membrana Spectra / MWCO: 6-8000) contra citrato de sódio 2,2 mM. Os PNB-PEG-NH2 foram acoplados ao éster NHD do IRDye® 680RD em tampão de bicarbonato (pH

8,1) durante 12 h à temperatura ambiente. O complexo de GNPs-PEG-IRDye foi então purificado por diálise (durante quatro dias numa membrana Spectra / MWCO: 6-8000) contra citrato de sódio 2,2 mM e a solução foi mudada duas vezes por dia.

Imagens de fluorescência ex vivo dos principais órgãos e quantificação

Ratas fêmeas BALB com 6 semanas de idade (n = 3-4). (Charles River, França) receberam injeção I.V de GNPs as três concentrações diferentes testadas (GNP1, GNP2 e GNP3). Após 48 h, todos os principais órgãos foram coletados para imagem de fluorescência *ex vivo*. As imagens foram adquiridas a 700 nm com uma resolução de 85 mm. Os dados foram analisados no software Pearl Impulse, versão 3.01 (LI-COR Biosciences, Lincoln, NE, EUA). A intensidade total da fluorescência foi determinada desenhando uma região de interesse (ROI).

4.11 - Atividade antioxidante das GNPs

O efeito antioxidante das GNPs foi avaliado através do consumo de GSH, formação de MDA e inibição da MPO. Amostras de fígado foram colhidas como descrito acima e armazenadas a -80º. Após homogeneização e centrifugação (2000 × g por 20 min), a atividade de MPO foi determinada por um método colorimétrico previamente descrito. Os resultados são relatados como unidades de MPO por grama de tecido.

Para quantificar o aumento de radicais livres na amostra hepática, o conteúdo de MDA foi medido pelo ensaio descrito por Araújo et all., 2016. As amostras de fado foram suspensas em tampão de Tris HCl 1: 5 (p/v) e picadas com uma tesoura durante 15s numa placa arrefecida com gelo. A suspensão resultante foi homogeneizada durante 2 min com um homogeneizador de Potter automático e centrifugada a 2500 x g a 4 durante 10 min. Os sobrenadantes foram utilizados para determinar o teor de MDA. Os resultados são expressos como nanomols de MDA por grama de tecido.

Os níveis de GSH nos tecidos do fígado foram medidos como antioxidantes. O conteúdo de GSH foi medido pelo ensaio descrito por[52-53]. Amostras de fígado (5 por grupo) foram armazenadas a - 80 °C até o uso. Homogenatos de tecido do fígado (0,25 mL de uma solução de tecido a 5%

preparada em 0,02 M de EDTA) foram adicionados a 320 mL de água destilada e 80 mL de TCA a 50%. As amostras foram centrifugadas a 3000 rpm durante 15 min a 4. O sobrenadante (400 mL) foi adicionado a 800 mL de tampão Tris 0,4 M a pH 8,9 e 20mL de DTNB 0,01 M. A absorbância de cada amostra foi medida a 420 nm e os resultados foram reportados como unidades de GSH por miligrama de tecido.

4.12 - Análise de citocinas

Amostras de fígado (três amostras por grupo) foram armazenadas a – 80 °C até o uso. O tecido foi homogeneizado e processado conforme descrito por[50]. Níveis de IL-1β (faixa de detecção: 62,5 - 4000 pg/mL; sensibilidade ou limite inferior de detecção [LLD]: 12,5 ng/mL de IL-1β recombinante de camundongo), IL-10 (faixa de detecção: 62,5 - 4000 pg/mL; sensibilidade ou LLD: 12,5 ng/mL de IL-10 de camundongo recombinante) e TNF - α (faixa de detecção: 62,5 – 4000 pg/mL; sensibilidade ou LLD: 50 ng/mL de TNF-α de camundongo recombinante) no fígado as amostras foram determinadas com um kit ELISA comercial (R & D Systems, Minneapolis, MN, EUA), como descrito anteriormente. Todas as amostras estavam dentro do comprimento de onda utilizado na espectrofotometria UV-VIS (absorbância medida a 490 nm).

4.13 - Análise histológica do parênquima hepático

As amostras de fígado foram fixadas em formol tamponado a 10%, desidratadas e embebidas em parafina. Secções de 5 µm de espessura foram obtidas para coloração com hematoxilina-eosina (H&E) e examinadas por microscopia de luz (40x, Nikon E200 LED). Três secções do fígado (seis animais por grupo) foram analisadas por dois patologistas. A patologia hepática foi classificada como se segue: esteatose (a porcentagem de células de fígado contendo gordura): < 25 % = 1, < 50 % = 2, < 75 % = 3, > 75 % = 4; inflamação e necrose foram analisadas contando-se os focos encontrados: 1 foco por campo de baixa potência; 2 ou mais focos. A patologia foi pontuada de maneira duplo-cega por um dos autores e por um especialista externo em patologia do fígado de roedores.

Os cortes histológicos foram corados pelo kit de coloração picrosirius red (1% de Sirius red em ácido pícrico saturado; EasyPath, Indaiatuba, Brasil) por

24 h, ou hematoxilina e eosina (Easypath) e examinados sob microscopia de luz (Nikon Eclipse 2000 equipado com Nikon DS- Fi2; Nikon Corporation, Tóquio, Japão). Para fins de análise quantitativa, foram analisados o conteúdo de colágeno, amostrados aleatoriamente em 200 amostras de microscópio de luz (200X) por espécime hepático, incluindo grandes veias centrolobulares e grandes espaços portas (≥ 150 mm). Cerca de 20 imagens de microscopia de luz polarizada usando um microscópio Olympus BX60 (Olympus, Tóquio, Japão) (200X) por espécime foram capturadas e analisadas usando um sistema de detecção de limiar de cor desenvolvido no ImageJ (National Institutes of Health). Controles positivos e negativos conhecidos foram incluídos em cada lote de amostras. A reatividade tecidual em todos os grupos (controle negativo, controle positivo e grupos tratado com GNPs) foi avaliada. Os valores são expressos como porcentagem da área positiva. As medidas do índice de contraste foram obtidas a partir da área selecionada x 100/área total posicionada através das regiões de interesse (três amostras por animal). Além disso, a fibrose hepática foi quantificada usando o sistema de pontuação de[54]: nível 0 indicando ausência de fibrose; o nível 1 indicou aumento da área do espaço porta; o nível 2 foi atribuído à expansão fibrosa da maioria das áreas do espaço porta; o nível 3 foi atribuído a lóbulos com expansão fibrosa da maioria das áreas do portal com portal ocasional para a ponte do portal; o nível 4 foi atribuído a lóbulos com expansão fibrosa da maioria das áreas do portais com ponte marcada; o nível 5 foi atribuído a lóbulos com ponte marcada (de um espaço porta a outro ou espaço porta para veia central) com nódulos ocasionais (cirrose incompleta); nível 6 para Cirrose nos lóbulos.

Coletou-se amostras de sangue do rato e centrifugou-se a 3000 g durante 10 min e os sobrenadantes resultantes foram utilizados para medir o nível de alanina aminotransferase no sangue (ALT), aspartato aminotransferase (AST) para avaliar a lesão hepática induzida pelo álcool. Utilizou-se solução de proteína citosólica do fígado para medir a concentração de triglicerídeos hepáticos (mg/g de proteína total do fígado) como marcador do excedente lipídico induzido pelo álcool no fígado. Os níveis de ALT, AST e triglicérides hepáticos foram medidos com um analisador automático (FDC4000; Fuji Medical Systems, Tóquio, Japão).

4.14 - Microscopia eletrônica de transmissão

Para avaliar a captação das GNPs pelas células hepáticas, foram retirados fragmentos de 0,5 cm das amostras de cada tratamento e foram criofixadas em Solução de Karnovisky (2,5%) e paraformaldeído (2,5%) em tampão de cacodilato 0,1 M por aproximadamente 4 horas 4ºC. Após a fixação, o material foi lavado com 4x cacodilato de sódio (15 min cada banho). Uma gota de 1,6% de Ferrocianeto de Potássio (FCK) e 2% de Tetróxido de Ósmio por 1 h em câmara escura foi adicionada, seguida por 2 lavagens com cacodilato de sódio 0,1 M por 15 min e duas lavagens com água destilada. Contraste “em bloco” com 0,5% de acetato de uranila em câmara escura por 2 h sob refrigeração, desidratado com acetona em diferentes concentrações, infiltrado e incluído em resina. As seções ultra-finas (1µm) são coradas com azul de toluidina e examinadas sob microscópio eletrônico de transmissão Zeiss, modelo EM 902 a 80Kv.

4.15 - Coloração Imuno-histoquímica

Cortes de fígado de 4 µm foram adicionados a cada grupo com micrótomo e transferidas para as lâminas revestidas com gelatina. Cada parte de tecido foi então desparafinizada e reidratada. Como as fibras de couro foram lavadas com Triton X-100 a 0,3% em fosfato e peroxidase endógena (peróxido de hidrogênio a 3%). As secreções teciduais foram incubadas durante a noite a 4ºC com anticorpos primários (Santa Cruz Biotecnologia, Interprise, Brasil) contra TGF-β, FGF, SOD-1, GPX-1 e IL-1β. Testes de diluição (3 diluições) foram realizados com todos os fragmentos para identificação de 1:800; 1:600; 1:800; 1:1000 e 1:600, respectivamente. As fibras foram lavadas com fosfato e incubadas com uma enzima conjugada com estreptavidina/HRP (Biocare Medical, Concord, CA, EUA) durante 30 min. A imunorreatividade às várias proteínas foi visualizada com um kit de detecção baseado em colorimetria seguindo o protocolo do fabricante pelo fabricante (TrekAvidin-HRP Label + Kit da Biocare Medical, Dako, EUA). As secções foram contrastadas com hematoxilina. Controles positivos foram incluídos em cada conjunto de amostras. Microscopia de planimetria (LED da Nikon E200, Departamento de Morfologia/UFRN) com objetiva de alta potência (40×) foi utilizada para marcar

uma restrição da imunomarcação celular: 1 = ausência de células positivas; 2 = Número mínimo de imagens positivas ou células isoladas; 3 = número moderado de células positivas; e 4 = grande número de células positivas. As análises foram avaliadas por dois examinadores treinados.

4.16 - Microscopia de Imuno-Fluorescência

Três seções de tecido de cada animal (seis animais por grupo) foram desparafinizadas em xilol e lavadas numa série de concentrações de etanol e PBS. A recuperação do antigênica foi realizada com citrato de sódio 10mM com Tween 20 a 0,05% durante 40 min a 95°C. O background da autofluorescência foi reduzido pela incubação das partes em 0,1% do Sudan Black em álcool a 70% por 40 min em temperatura ambiente. As secções foram incubadas durante a noite com os anticorpos primários anti-IL-1β, TNF-β e MIF (1: 200, 1: 400 e 1: 400 Abcam, EUA e Santa Cruz Biotechnology, EUA, respectivamente), em solução de bloqueio 1% de soro de cabra normal; Abcam, USA e Santa Cruz Biotecnologia, EUA, respectivamente), lavadas com PBS 0,2% triton X-100 durante 5 min e incubadas com anticorpo conjugado de cabra com Alexa Fluor 488 (1:500 em BSA 1%) e contra coloração nuclear DAPI (Sigma, EUA). Finalmente, como as seções foram montadas com o meio Vecta shield. Imagens fluorescentes foram obtidas conforme descritas por[50].

4.17 – Análise da Expressão de proteínas através de Western blot

Os fragmentos de tecido foram macerados em nitrogênio líquido e seguido de adição do tampão de RIPA (25 mM Tris-HCL, pH 7,6; 150 mM NaCl; 5 mM EDTA; 1% NP40; 1% triton X-100; 1% de sódio desoxicolato; 0,1% SDS) e inibidor de protease (1 de inibidor: 100 de RIPA). Para extração de proteínas as amostras foram centrifugadas (17 min, 4x a 13000 RPM) e o sobrenadante foi recolhido. As moléculas de proteína foram separadas através do ensaio de ácido (Thermo Fisher Scientific) de acordo com o protocolo do fabricante. Um gel de poliacrilamida-SDS (10% ou 8%) foi utilizado com 50 µm de proteína (preparado anteriormente com tampas de amostra, BioRad e desnaturado a 95 durante 5 min). Em seguida, a proteína foi transferida para uma membrana de PVDF (BioRad) por 2 h, bloqueada com 5% de BSA por 1 h, incubada durante a noite com um anticorpo primário (camundongo anti-β

actina, sc-81178, 1:500, Santa Cruz Biotecnologia anti-TGF-β, sc 80346 de rato, 1:200, Biotecnologia Santa Cruz, anti-ERK1/ERK2 de rato, 136200, 1:500, Invitrogen, anti-Iba-1 de cabra, ab107159 Abcam), um anticorpo secundário (anti-coelho de cabra, 656120, Invitrogen, 1:1000, IgG anti-murino de cabra, 626520, Invitrogen, 1:500, ou anti-cabra de coelho, A16142, Invitrogen, 1:1000) durante 1 he 30 min. As membranas foram incubadas utilizando o sistema ECL de acordo com as instruções do fabricante (BioRad) e o sinal de quimiluminescência foi detectado utilizando o sistema ChemiDocTM XRS (BioRad). A quantificação densitométrica das bandas foi realizada através do software ImageJ (NIH, Bethesda, MD, EUA).

4.18 - Análise da expressão de mRNA

O RNA total foi extraído do tecido do fígado com reagente trizol (Invitrogen Co. USA) e o Sistema de Isolamento de RNA Total SV (Promega, Madison, WI). O DNAc de primeira cadeia foi sintetizado a partir de 1 µg de RNA total com o Sistema de Transcriptase Reversa ImProm-IITM para RT-PCR (Promega), de acordo com o protocolo do fabricante. Análises de PCR quantitativa em tempo real dos mRNAs de GAPDH, PCI, PCIII, NF-Kβ, F4/80, AKT e PI3K foram realizadas com SYBR Green Mix no sistema Applied Biosystems 17500 FAST (Applied Biosystems, Foster City, CA), de acordo com um protocolo padrão com os seguintes primers da tabela 1.

O gene de referência para normalização foi selecionado de uma análise de 18S (sequência GenBank NM_003286.2), ubiquitina C (UBC, NM_021009.4), β-actina (ACTB, NM_001101.3) e gliceraldeído-3-fosfato desidrogenase (GAPDH, NM_002046.3) genes. GAPDH foi escolhido como o gene de referência porque não apresentou diferentes padrões de amplificação[55]. Como é um gene constitutivo para eucariotos, o gene de referência não deve ser modificado na doença.

Todas as análises foram realizadas em um instrumento PCR de tempo real rápido 7500 (Applied Biosystems, CA, EUA). As condiçõeses padrões de PCR foram as seguintes: 50 ºC durante 2 min e 95 ºC durante 10 min, seguido por quarenta ciclos de 30 s a 94 ºC uma temperatura de iniciador de hibridação variável durante 30s e 72ºC durante 1 min. As reações foram realizadas em duplicata, de acordo com o protocolo padrão de PCR TaqMan® (Applied

Biosystems, Foster City, CA, EUA) em um volume total de 10 µL contendo aproximadamente 20 ng de cDNA. Valores médios de CT foram usados para calcular os níveis relativos de expressão dos genes alvo para os grupos experimentais, em relação àqueles no grupo controle negativo; os dados de expressão foram normalizados em relação ao gene de manutenção GAPDH usando a fórmula $2^{-\Delta\Delta Ct}$.

4.19 - Análise estatística

Os dados são apresentados como médias com seus erros padrão (SEM) ou como medianas. A análise de variância (ANOVA) seguida do teste de Bonferroni foi usada para testes paramétricos. Os testes de Kruskal-Wallis e Dunn foram utilizados para comparar medianas para testes não paramétricos (Graph Pad Prism 5.0 Software, La Jolla, CA, EUA).

5 - ARTIGOS PUBLICADOS

1 – Anti-inflammatory, analgesic and anti-tumor properties of gold nanoparticles. de Araújo, Raimundo Fernandes; de Araújo, Aurigena Antunes; Pessoa, Jonas Bispo; Freire Neto, Franscisco Paulo; da Silva, Gisele Ribeiro; Leitão Oliveira, Ana Luiza C.S.; **de Carvalho, Thaís Gomes**; Silva, Heloiza F.O.; Eugênio, Mateus; Sant'anna, Celso; Gasparotto, Luiz H.S. doi: 10.1016/j.pharep.2016.09.017

O artigo foi publicado no periódico: Pharmacological Reports, que possui fator de impacto 2.787 e Qualis B1 para Medicina II.

2 – Gastroprotective and Antioxidant Activity of *Kalanchoe brasiliensis* and *Kalanchoe pinnata* Leaf Juices against Indomethacin and Ethanol-Induced Gastric Lesions in Rats. de Araújo, Edilane; Guerra, Gerlane; Araújo, Daline; de Araújo, Aurigena; Fernandes, Júlia; de Araújo Júnior, Raimundo; Da Silva, Valéria; **de Carvalho, Thaís Gomes**; Ferreira, Leandro; Zucolotto, Silvana.; doi: 10.3390/ijms19051265

O artigo foi publicado no periódico: International Journal of Molecular Sciences, que possui fator de impacto 3.678 e Qualis A2 para Medicina II.

3 - Spherical neutral gold nanoparticles improve anti-inflammatory response, oxidative stress and fibrosis in alcohol-methamphetamine-induced liver injury in rats. de Carvalho TG[1], Garcia VB[1], de Araújo AA[2], da Silva Gasparotto LH[3], Silva H[3], Guerra GCB[2], de Castro Miguel E[4], de Carvalho Leitão RF[5], da Silva Costa DV[5], Cruz LJ[6], Chan AB[7], de Araújo Júnior RF[8]. International Jornal os Phamaceutics.; 2018 Jun 7;548(1):1-14. doi: 10.1016/j.ijpharm.2018.06.008.

O artigo foi aceito para publicação no periódico: International Jornal os Phamaceutics, que possui fator de impacto 3.862 e Qualis A2, tem data prevista para publicação em setembro de 2018 para Medicina II.

6 - COMENTÁRIOS, CRÍTICAS E SUGESTÕES

Os resultados apresentados aqui fazem referência a proposta inicial apresentada durante o processo seletivo, algumas modificações foram feitas para melhorar a proposta inicial, na qual adicionamos algumas metodologias a fim de melhorar o delineamento do estudo e responder todos os questionamentos que surgiram durante o estudo bem como atender as demandas dos revisores da revista que aceitou o nosso estudo.

Esse trabalho merece mérito pela originalidade com que foi executado diante das dificuldades metodológicas que tivemos para concluir, além da diversidade de pessoas de diferentes áreas envolvidas que contribuíram de formas diferentes para a conclusão do mesmo.

Todo o processo que resultou na conclusão do Mestrado foi de grande contribuição para formação e evolução intelectual, as disciplinas como Bioética e Redação do trabalho científico são de grande relevância talvez as mais importantes dentre todas as outras cursadas, o estágio de docência foi um grande desafio, mas crucial para me preparar para os desafios que enfrentarei como docente.

As metas que tracei inicialmente foram atingidas ao concluir esse grande passo na minha vida, e ao concluir vejo que o Metrado é apenas o começo e para esse amadurecimento científico, uma grande meta foi traçada ao concluir esta, o Doutorado é o próximo grande passo para contribuir para minha formação docente.

Durante a formação de mestre tive a oportunidade de me inserir em outros grupos de pesquisa de áreas diferentes o que é de grande relevância para formação docente.

Durante dois anos contribui para a publicação de 3 artigos científicos, e outros que estão em fase de conclusão e deverão ser publicados ainda este ano. Ministrei um mini-curso para divulgar os trabalhos realizadas em nosso grupo de pesquisa.

International Journal of Pharmaceutics 548 (2018) 1–14

Contents lists available at ScienceDirect

International Journal of Pharmaceutics

journal homepage: www.elsevier.com/locate/ijpharm

Spherical neutral gold nanoparticles improve anti-inflammatory response, oxidative stress and fibrosis in alcohol-methamphetamine-induced liver injury in rats

Thaís Gomes de Carvalho[a,c], Vinícius Barreto Garcia[a,c], Aurigena Antunes de Araújo[d], Luiz Henrique da Silva Gasparotto[e], Heloiza Silva[e], Gerlane Coelho Bernardo Guerra[d], Emilio de Castro Miguel[f], Renata Ferreira de Carvalho Leitão[g], Deiziane Viana da Silva Costa[g], Luis J Cruz[h], Alan B. Chan[i], Raimundo Fernandes de Araújo Júnior[a,b,c,*]

[a] Department of Morphology, Federal University of Rio Grande do Norte, Natal 59072-970, RN, Brazil
[b] Post-Graduation Programme in Structural and Functional Biology, Federal University of Rio Grande do Norte, Natal 59072-970, RN, Brazil
[c] Post-Graduation Programme in Health Science, Federal University of Rio Grande do Norte, Natal 59072-970, RN, Brazil
[d] Department of Biophysics and Pharmacology, Post-Graduation Programme in Public Health, Post-graduation Programme in Pharmaceutical Science, Federal University of Rio Grande do Norte, Natal 59072-970, RN, Brazil
[e] Group of Biological Chemistry and Chemometrics, Institute of Chemistry, Federal University of Rio Grande do Norte, Natal 59072-970, RN, Brazil
[f] Department of Physical/Analytical Center/UFC, Fortaleza, CE, Brazil
[g] Department of Morphology/Post-graduate Program in Morphology/UFC, Fortaleza, CE, Brazil
[h] TranslationalNanobiomaterials and Imaging, Department of Radiology, Leiden University Medical Center, 2333 ZA Leiden, The Netherlands
[i] Percuros B.V, 2333 CL Leiden, The Netherlands

ARTICLE INFO

Keywords:
Gold nanoparticles
Ethanol
Methamphetamine
Toxicity and Kupffer cells

ABSTRACT

This study aimed to elucidate the anti-inflammatory, anti-oxidant and antifibrotic effects of gold nanoparticles (GNPs) in rats subjected to liver injury with ethanol and Methamphetamine (METH). The liver injury was induced by gavage administrations of 30% alcoholic solution (7 g/kg) once a day during 28 days, followed by METH (10 mg/kg) on the 20th and 28th days of treatment. GNPs treatment (724.96 μg/kg) during the ethanol and METH exposure was associated with reduced steatosis, hepatic cord degeneration, fibrosis and necrosis. Furthermore, there was a reduction in biochemical markers of liver damage and oxidative stress, and pro-inflammatory cytokines IL-1β and TNF-α, compared to ethanol + METH group alone. A decrease of FGF, SOD-1 and GPx-1 expression was also observed. GNPs down-regulated the activity of Kupffer cells and hepatic stellate cells affecting the profile of their pro-inflammatory cytokines, oxidative stress and fibrosis through modulation of signaling pathways AKT/PI3K and MAPK in ethanol + METH-induced liver injury in a rat model.

1. Introduction

Many drugs, including alcohol and stimulants, are used in social contexts, perhaps because they enhance prosocial behaviors such as social bonding, talking, and empathy (Kirkpatrick and De Wit, 2013; Sayette et al., 2012). Poly-substance use is a term coined to denote the concomitant or sequential consumption of more than one psychoactive drug over an interval of at least 12 months for either therapeutic or recreative purposes. Amongst the substances that are co-administered with illicit drugs, ethanol is undoubtedly the most prevalent chemical responsible for the increasing number of hospital admissions and deaths (Winkler et al., 2016). Ethanol is frequently co-used with psychostimulant drugs such as methamphetamine (METH) or cocaine (Kedia et al., 2007) in order to enhance and prolong the drug effects.

Evidence suggests that the co-administration of ethanol and cocaine produces amplified and extended subjective effect (Ikegami et al., 2002), fewer studies have examined the somatic impact of the METH-ethanol combination in brain (Zendulka et al., 2012; Almalki et al., 2018; Wells et al., 2016). Concerning toxic effects on liver, (Koriem and Soliman, 2014) found that a hoop of edema in the periportal area compresses the surrounding hepatocytes, leading to formation of hyperemic vessels. The association of ethanol and METH produces a variety of histological abnormalities in liver such as abundant cytoplasmic lipid droplets diffusely distributed along the lobules. Besides, a

*Corresponding author: Federal University of Rio Grande do Norte, Lagoa Nova, SN, 1524 Natal, Brazil.
E-mail address: araujojr@cb.ufrn.br (R.F. de Araújo Júnior).

https://doi.org/10.1016/j.ijpharm.2018.06.008
Received 16 February 2018; Received in revised form 24 May 2018; Accepted 4 June 2018
Available online 07 June 2018
0378-5173/

Spherical neutral Gold nanoparticles improve anti-inflammatory response, oxidative stress and fibrosis in alcohol-methamphetamine-induced liver injury in rats

Thaís Gomes de Carvalho[a,c], Vinícius Barreto Garcia[a,c], Aurigena Antunes de Araújo[d], Luiz Henrique da Silva Gasparotto[e], Heloiza Silva[e], Gerlane Coelho Bernardo Guerra[d], Emilio de Castro Miguel[f], Renata Ferreira de Carvalho Leitão[g], Deiziane Viana da Silva Costa [g], Luis J Cruz[h], Alan B. Chan[i], Raimundo Fernandes de Araújo Júnior[a,b,c]

Present addresses:

[a] Department of Morphology, Federal University of Rio Grande do Norte, Natal 59072-970, RN, Brazil

[b] Post-Graduation Programme in Structural and Functional Biology, Federal University of Rio Grande do Norte, Natal 59072-970, RN, Brazil

[c] Post-Graduation Programme in Health Science, Federal University of Rio Grande do Norte, Natal 59072-970, RN, Brazil

[d]Department of Biophysics and Pharmacology, Post-Graduation Programme in Public Health, Post-graduation Programme in Pharmaceutical Science, Federal University of Rio Grande do Norte, Natal 59072-970, RN, Brazil

[e]Group of Biological Chemistry and Chemometrics, Institute of Chemistry, Federal University of Rio Grande do Norte, Natal 59072-970, RN, Brazil

[f]Department of Physical/Analytical Center/UFC, Fortaleza, CE, Brazil

[g]Department of Morphology/Post-graduate Program in Morphology/UFC, Fortaleza, CE, Brazil

[h]Translational Nanobiomaterials and Imaging, Department of Radiology, Leiden University Medical Center,2333 ZA Leiden, The Netherlands

[i]Percuros B.V., 2333 CL Leiden, The Netherlands

ABSTRACT

This study aimed to elucidate the anti-inflammatory, anti-oxidant and antifibrotic effects of gold nanoparticles (GNPs) in rats subjected to liver injury with ethanol and Methamphetamine (METH).The liver injury was induced by gavage administrations of 30% alcoholic solution (7 g/kg) once a day during 28 days, followed by METH (10 mg/kg) on the 20th and 28th days of treatment. GNPs treatment (724.96 µg/kg) during the ethanol and METH exposure was associated with reduced steatosis, hepatic cord degeneration, fibrosis and necrosis. Furthermore, there was a reduction in biochemical markers of liver damage and oxidative stress, and pro-inflammatory cytokines IL-1β and TNF-α, compared to ethanol + METH group alone. A decrease of FGF, SOD-1 and GPx-1 expression was also observed. GNPs *down-regulated the activity of Kupffer cells and* hepatic stellate cells *affecting the profile of their pro-inflammatory cytokines, oxidative stress and fibrosis through modulation of signaling pathways AKT/PI3K and MAPK* in ethanol + METH-induced liver injury in a rat model.

Keywords: *Gold nanoparticles, ethanol, methamphetamine, toxicity and Kupffer cells.*

1. INTRODUCTION

Many drugs, including alcohol and stimulants, are used in social contexts, perhaps because they enhance prosocial behaviors such as social bonding, talking, and empathy (Kirkpatrick and De Wit 2013; Sayette et al. 2012). Poly-substance use is a term coined to denote the concomitant or sequential consumption of more than one psychoactive drug over an interval of at least 12 months for either therapeutic or recreative purposes. Amongst the substances that are co-administered with illicit drugs, ethanol is undoubtedly the most prevalent chemical responsible for the increasing number of hospital admissions and deaths (Winkler et al. 2016). Ethanol is frequently co-used with psychostimulant drugs such as methamphetamine (METH) or cocaine (Kedia, Sell, and Relyea 2007) in order to enhance and prolong the drug effects.

Evidence suggests that the co-administration of ethanol and cocaine produces amplified and extended subjective effect (Ikegami et al. 2002), fewer studies have examined the somatic impact of the METH-ethanol combination in brain (Zendulka et al. 2012; Almalki et al. 2018; Wells et al. 2016).Concerning toxic effects on liver, (Koriem and Soliman 2014) found that a hoop of edema in the periportal area compresses the surrounding hepatocytes, leading to formation of hyperemic vessels. The association of ethanol and METH produces a variety of histological abnormalities in liver such as abundant cytoplasmic lipid droplets diffusely distributed along the lobules. Besides, a pronounced deposition of collagen fibers between the hepatocytes and the endothelial cells of the sinusoids results in an apparent reduction of the size and density of the hepatocytes in the sinusoids and in the bile canaliculi (Pontes et al. 2008).

Three mechanisms have been proposed for alcoholic liver injury: (i) acetaldehyde toxicity (Guo, Zhong, and Ren 2009); (ii) metabolic generation of reactive oxygen species (ROS) or exposure to oxidative stress (Yin et al. 2009; Tang et al. 2014); and (iii) oxidative stress in hepatocytes caused by immune response (Chen et al. 2011; Park et al. 2013). The latter has been found in alcoholic-liver-injury patients (Chen et al. 2011), which helps prevent ethanol-induced liver disease.

In liver injury, activated Kupffer cells release a number of soluble agents, including cytokines, such as TGF-β, and TNF-α, ROS (Kang et al. 2008) and factor nuclear kappa B (NF-κB) translocates to the nucleus, in which it binds to the promoter of target genes such as TNF-α and other pro-inflammatory cytokines (Son et al. 2011). These factors act on hepatic stellate cell (HSC), which are localized in the parasinusoidal space (Wen et al. 2013). The activated phosphatidylinositol-4,5-bisphosphate 3-kinase (PI3-K) participate in regulation of HSC migration, proliferation, collagen secretion and adhesion(Friedman 2000) besides being involved in regulating a number of cellular responses, such as cell growth, survival and migration. The protein kinase B (Akt or PKB) is downstream of PI3-K and activation of Akt is associated with HSC proliferation and α1 (I) collagen transcription and translation (Reif et al. 2003).

Functionalized spherical gold nanoparticles (GNPs) with controlled geometrical and optical properties are the subject of intensive studies and biomedical applications, including genomics, biosensorics, immunoassay (Bartneck, Warzecha, and Tacke 2014; He et al. 2008), clinical chemistry (Bartneck, Warzecha, and Tacke 2014), laser phototherapy of cancer cells (Gunes et al. 2010), the targeted delivery of drugs (Aslan, Lakowicz, and Geddes 2004), DNA and antigens (Dykman and Bogatyrev 2000), optical bioimaging and the monitoring of cells (Hirsch et al. 2003) and tissues with the use of state-of-the-art detection systems.

Investigation of GNPs cytotoxicity focuses on their size, shape, doses and surrounding ligands being those chemically positive and negative charged responsible for causing cell damages through oxidative alterations in mitochondrial membrane potential (De and Rotello 2008; Schaeublin et al. 2011). Spherical neutral GNPs are more suitable for biomedical application due to the their inability in removing electrons from molecules, such as membrane lipids and mitochondria, as well as generating free radicals (Loumaigne et al. 2010; Fröhlich 2012). Local macrophages like kupffer cells ingest foreign materials such as pathogens and nanoparticles, and recruit additional macrophages to the inflamed microenvironment, producing cytokines including TNF-α, IL-6 and TGF-β that up-regulate the inflammatory process (Tilg and Moschen 2008). Positively charged nanoparticles are preferentially taken up by monocyte-derived macrophages and Kupffer cells that

have an M2-like phenotype which produce high level of TGF-β (Mac Parland et al. 2017).

In this context, macrophages like Kupffer cells therefore not only represent attractive targets for nanomedicine in liver disease, but they also need to be considered as potential particle scavenging cells in any kind of parenteral nanoparticle administration. As such, changing local Kupffer cell behavior may affect the progress of inflammation-related disorders. Therefore, the aim of the present work was to evaluate the anti-inflammatory, antioxidant and antifibrotic effect of GNP in an animal model of ethanol and METH-induced liver injury through an analysis of several markers.

2. METHODS

Chemicals

The absolute ethyl alcohol (PA 99.8%) was obtained from Vetec Quimica, Brazil. Methamphetamine (METH) was acquired from Fisher Scientific, according to the law 10.357 of December 27, 2001, which establishes rules for production, control and inspection of chemical substances.

Murine macrophage cells (RAW 264.7; cat. no.TIB-71) were obtained from American Type Culture Collection (Manassas, VA, USA). Dulbecco's modified Eagle's medium (DMEM) was purchased from Invitrogen Corporation (Carlsbad, CA, USA); fetal bovine serum from Hyclone Company (Logan, UT, USA).

Antibodies anti-TGF- β, FGF, SOD-1, GPX, IL-1β, TNF-β and MIF were obtained from Santa Cruz Biotechnology Enterprise, Brazil. Streptavidin-HRP-conjugated secondary antibody (Biocare Medical, Concord, CA, USA), TrekAvidin-HRP Label + Kit (Biocare Medical, Dako, USA), IL-1β, IL-10, TNF-α and ELISA kit (R&D Systems, Minneapolis, MN, USA) were also utilized in this study.

Cell culture

RAW 264.7 macrophage cells were grown in DMEM medium with 10% fetal bovine serum. Cells were seeded at a density of $5x10^4$ cells per well in 6-well plates and reached 50-60% confluence 24-h after seeding, just before exposure to the non-cytotoxic concentration of GNPs in 10μg/mL for treatment (Q. Zhang et al. 2011). The

cells were maintained in a 5% CO^2 incubator at 37ºC and 95% humidified air. Cells were subsequently analysed by a phase-contrast microscope.

Immunofluorescence

RAW 264.7 macrophage cells were plated onto glass coverslips in 24 well plates (5×10^4 cells/well) and allowed to grow for 24 h. The cells were then washed, fixed with 1% paraformaldehyde, permeabilized with Triton-X and incubated with 100 µL of GNPs and 4',6-diamidino-2-phenylindole was used for nuclear stainingfor 10 minutes in a humid atmosphere at room temperature. Control experiments were performed under the same conditions but without GNPs addition. The glass coverslips were then directly observed with the Leica DM5500 B fluorescence microscope (filter settings: TXR, Cy7, FITC and DAPI), equipped with a condenser using laser excitation from 512 to 542 nm.

Animal

Thirty six Wistar rats male weighing between 270 g and 300 g, obtained from the animal house of Department of Biophysical and Pharmacology – Federal University of Rio Grande do Norte (UFRN), Natal, Brazil, were randomly divided into six groups of six animals each and used for experiments. Animals were housed in cages with free access to food and water at temperature and humidity controlled environment under a 12 h light/dark cycle. Animals were treated according to the ethical principles for animal experimentation. All experiments were approved by UFRN Ethics Committee (approval number: 018/2015).

Preparation and administration of ethanol

7 g per kg body weight of 30% v/v ethanol solution was used as chronic dose in this experiment and 30 g of absolute ethanol was dissolved in distilled water and made up to 100 ml, then 6.2 ml of the solution was daily administered for 28 days to each rat treated with ethanol (de Araújo et al. 2016).

Preparation and administration of methamphetamine

We used the dose of 10 mg/kg for METH, in which 25 mg of METH were diluted in 10 ml of distilled water. Each animal received 0.1 ml of this solution, which corresponds to 2.5 mg in each dose (Halpin, Gunning, and Yamamoto 2013).

Production of gold nanoparticles

Gold nanoparticles (GNPs) were obtained from a partnership with the Department of Chemistry of the Federal University of Rio Grande do Norte-UFRN, Brazil. These GNPs are produced as described by (Gasparotto et al. 2012).

First, Au^{3+} was reduced by glycerol in alkaline medium and polyvinylpyrrolidone was used to stabilize the gold nanoparticles. Diluted HCl was then added to bring the solution pH to 7 and generate neutral GNPs. Considering the quantitative transformation of gold ions into nanoparticles, the concentration of GNPs was estimated to be 197 $\mu g/mL^{-1}$. The final mixture has a dark-red color due to the GNPs formation of 7.4 ± 1.6 nm in size.

A Zeta-Meter 3.0 + system (Zeta-Meter Inc., USA) at a temperature of 25 ± 2°C was used to determine the electrophoretic mobility of the GNPs colloidal solution (20 mL). The zeta potential was calculated using the Smoluchowski equation:

$$\zeta = \frac{\mu_E \eta_0}{\varepsilon_0 \varepsilon_r},$$

Where μ_E is the electrophoretic mobility, η_0 is the continuous phase viscosity, ε_0 is the permittivity of a vacuum, and $_r$ is the relative permeability of the continuous phase.

Dosage and administration of gold nanoparticles

The doses of GNPs were chosen through a pilot project, the doses of 700 µg/kg, 1000 µg/kg and 1.500 µg/kg were tested. The dose 700 µg/kg showed best results in decreased inflammatory cytokines IL-1β and TNF-α (de Araújo et al. 2017). The dose of 700 µg / kg was used to calculate the doses to be used in the experiment, based on a gold nanoparticle formulation with a concentration of 197 µg / mL^{-1}.

The doses were adjusted so that for all groups treated by the oral route by gavage the final volume used was standardized in 1ml. In order to evaluate the dose-dependent effect, the doses were fractionated into 3: starting with the highest dose:

724.96 µg/kg (GNP3); an intermediate dose corresponding to 362.48 µg/kg (GNP2); and finally the third dose with the lowest concentration: 181.48 µg/kg (GNP1).

Induction of ethanol and METH-induced liver injury

The protocol for hepatic injury induction by exposure to alcohol and METH is summarized below:

1) Animals were treated with GNP1, GNP2 and GNP3 one hour before ethanol administration (30%, 7g/kg) by oral gavage. Each treatment had three doses to be tested: 181.48 µg/kg, 362.48 µg/kg and 724.96 µg/kg, respectively.

2) Saline solution (NaCl 0.9%) was administered by oral gavage once a week every six days during the first and second week of hepatic injury induction. Methamphetamine was administrated by oral gavage on the 3rd and 4th weeks in place of the saline solution. Saline/Methamphetamine were administered by oral gavage3 hours after ethanol. In the non-methamphetamine groups, saline solution was used by oral gavage to simulate the methamphetamine in the 3rd and 4th week.

3) Step 1 was repeated 7 days a week during 28 days.

4) Step 2 was repeated once a week every 7 days until the end of 28 days of injury induction.

Euthanasia was performed on the 29th day by intraperitoneal injection of Ketamine 7.5 ml/kg (50 mg/ml) and Xylazine 2.5 ml/kg (20 mg/ml). All animal groups were fasted for 12 h to perform the subsequent biochemical analysis. Once unconscious, the animals underwent cardiac puncture followed by removal of the liver.

Liver fragments were frozen at -80°C for cytokine and oxidative stress analysis, Western blot quantification, qPCR and ultra-structural evaluation using the Transmission Electron Microscopy technique. Other liver fragments were immersed in 10% buffered formalin for histopathological Analysis.

Biodistribution of gold nanoparticles

Conjugation of near-infrared (NIR) fluorescence to the GNPs

Firstly, GNPs were conjugated to the thiol group of the alpha-amino-omega-mercapto poly (ethylene glycol) hydrochloride (SH-PEG-NH2, MW 3.000 g/mol) during 3 h at room temperature. The excess of non-conjugated SH-PEG-NH2 was

removed by dialysis (for three days in a membrane Spectra/MWCO: 6-8000) against sodium citrate 2.2 mM. The GNPs-PEG-NH2 were coupled to the IRDye® 680RD NHS ester in bicarbonate buffer (pH 8.1) during 12 h at room temperature. The GNPs-PEG-IRDye complex was then purified by dialysis (for four days in a membrane Spectra/MWCO: 6-8000) against sodium citrate 2.2 mM and the solution was changed two times a day.

Ex vivo fluorescence imaging of major organs and quantification

6 weeks oldfemale BALB/c mice (n = 3-4) (Charles River, France) were sacrificed after 48 h of intravenous injection (I.V) of the GNPs at three different concentrations (GNP1; GNP2 and GNP3). After 48 h, all major organs were excised for *ex vivo* fluorescence imaging. Images were acquired 700 nm at a resolution of 85 mm. The data were analyzed using Pearl Impulse software, version 3.01 (LI-COR Biosciences, Lincoln, NE, USA). Total fluorescence intensity was determined by drawing a region of interest (ROI). The size and shape of the ROI was the same.

Antioxidant activity of GNPs

The antioxidant effect of GNPs was evaluated through the GSH consumption, MDA formation and MPO inhibition. Liver samples were harvested as described above and stored at −80°C until required for assay. After homogenisation and centrifugation (2000 × *g* for 20 min), MPO activity was determined by a previously described colorimetric method (De Araújo et al. 2016). Results are reported as units of MPO per gram of tissue.

To quantify the increase in free radicals in the liver sample, MDA content was measured via the assay described by (Esterbauer and Cheeseman 1990). Liver samples were suspended in buffer Tris HCl 1:5 (w/v) and minced with scissors for 15 sec on an ice-cold plate. The resulting suspension was homogenised for 2 min with an automatic Potter homogenizer and centrifuged at 2500 × g at 4°C for 10 min. The supernatants were assayed to determine MDA content. The results are expressed as nanomoles of MDA per gram of tissue.

GSH levels in the liver tissues were measured to antioxidant. GSH content was measured via the assay described by (de Araújo et al. 2017). Liver samples (5 per group) were stored at 70°C until use. Liver tissue homogenates (0.25 mL of a 5% tissue solution prepared in 0.02 M EDTA) were added to 320 mL of distilled water and 80 mL of 50% TCA. Samples were centrifuged at 3000 rpm for 15 min at 4°C.

The supernatant (400 mL) was added to 800 mL of 0.4 M Tris buffer at pH 8.9 and 20 µL of 0.01 M DTNB. The absorbance of each sample was measured at 420 nm, and the results were reported as level of GSH per milligram of tissue.

Cytokine Analysis

Liver samples (three samples per group) were stored at −80°C until use. The tissue was homogenized and processed as described by (Safieh-Garabedian et al. 1995). Levels of IL-1β (detection range: 62.5–4000 pg/mL; sensitivity or lower limit of detection [LLD]: 12.5 ng/mL of recombinant mouse IL-1β), IL-10 (detection range: 62.5–4000 pg/mL; sensitivity or LLD: 12.5 ng/mL of recombinant mouse IL-10) and TNF-α (detection range: 62.5–4000 pg/mL; sensitivity or LLD: 50 ng/mL of recombinant mouse TNF-α) in the intestinal samples were determined with a commercial ELISA kit (R&D Systems, Minneapolis, MN, *USA*), as described previously. All samples were within the wavelength used in UV-VIS spectrophotometry (absorbance measured at 490 nm).

Histological analysis from hepatic parenchyma

Liver samples were fixed in 10% neutral buffered formalin, dehydrated and embedded in paraffin. Sections of 5 µm thickness were obtained for hematoxylin–eosin staining (H&E) and examined by light microscopy (40x, Nikon E200 LED). Three sections of liver (six animals per group) were analyzed by two pathologists. Liver pathology was scored as follows: steatosis (the percentage of liver cells containing fat): <25% = 1, 25-50% = 2, 50-75% = 3, >75% = 4.; inflammation and necrosis: 1 focus per low-power field; 2 or more foci. Pathology was scored in a blinded manner by one of the authors and by an outside expert in rodent liver pathology (Nanji, Mendenhall, and French 1989). The main values of scores were used for statistical analysis.

Histological sections were stained using picrosirius red staining kit (1% Sirius red in saturated picric acid; EasyPath, Indaiatuba, Brazil) for 24 h, or haematoxylin and eosin (Easypath) and examined under light microscopy (Nikon Eclipse 2000 equipped with Nikon DS-Fi2; Nikon Corporation, Tokyo, Japan). For the purpose of quantitative analysis the collagen content, randomly sampled two hundred light microscope images (200X) per liver specimen, including large centrilobular veins and large portal tracts (≥150 mm) were analyzed. About 20 polarized light microscopy

images using an Olympus BX60 microscope (Olympus, Tokyo, Japan) (200X) per specimen were captured and analyzed using a color threshold detection system developed in ImageJ (National Institutes of Health). Known positive and negative controls were included in each batch of samples. Tissue reactivity in all groups (negative control, alcohol group and treated group with GNPs) was assessed. Values are expressed as percentage of positive area. Contrast index measurements were obtained from selected area x 100/total area positioned across the regions of interest (three samples per animal). Moreover, hepatic fibrosis was quantified using by (Ishak et al. 1995) scoring system: level 1 indicating the absence of fibrosis; level 2 indicated enlargement of portal area; level 3 was assigned to fibrous expansion of most portal areas; level 4 was assigned to lobules with fibrous expansion of most portal areas with occasional portal to portal bridging; level 5 was assigned to lobules with fibrous expansion of most portal areas with marked bridging (portal to portal and portal to central); level 6 was assigned to lobules with marked bridging (portal to portal and portal to central) with occasional nodules (incomplete cirrhosis); level 7 was observed Cirrhosis in the lobules.

Blood samples collected from the rat and were centrifuged at 3000 *g* for 10 min, and resultant supernatants were used to measure the blood alanine aminotransferase level (ALT), aspartate aminotransferase (AST) to evaluate the alcohol-induced liver injury. Liver cytosolic protein solution was used to measure the hepatic triglyceride concentration (mg/g total liver protein, % of control) as a marker of the alcohol-induced lipid surplus in the liver. The levels of ALT and hepatic triglyceride were measured with an automatic analyzer (FDC4000; Fuji Medical Systems, Tokyo, Japan). The data is presented as means with their standard errors (SEM).

Transmission electronic microscopy

In order to evaluate the uptake of the GNPs by hepatic cells, 0.5 cm fragments were taken from samples of each treatment and fixed in Karnovisky Solution (2.5%) and paraformaldehyde (2.5%) in buffer of 0.1 M cacodylate) for approximately 4 h at 4°C. After fixation the material was washed with 4x sodium cacodylate (15 min each bath). A drop of 1.6% Potassium Ferrocyanide (FCK) and 2% Osmium Tetroxide for 1 h in a darkroom was added, followed by 2 washes with 0.1 M sodium cacodylate for

15 min and two washes with distilled water. “In block” contrast with 0.5% uranyl acetate in a darkroom for 2 h under refrigeration, dehydrated with acetone in different concentrations, infiltrated and included in resin. Ultra-thin sections (1µm) are stained with toluidine blue and examined under Zeiss transmission electron microscope, model EM 902 at 80Kv.

Immunohistochemical staining

Thin sections of liver (4 µm) were obtained from each group with a microtome and transferred to gelatine-coated slides. Each tissue section was then deparaffinised and rehydrated. The liver tissue slices were washed with 0.3% Triton X-100 in phosphate buffer (PB) and quenched with endogenous peroxidase (3% hydrogen peroxide). Tissue sections were incubated overnight at 4°C with primary antibodies (Santa Cruz Biotechnology, INTERPRISE, Brazil) against TGF- β, FGF, SOD-1, GPX-1 e IL-1β. Dilution tests (3 dilutions) were performed with all antibodies to identify the 1:800; 1:600; 1:800; 1:1000 and 1:600, dilutions as appropriate, respectively. Slices were washed with phosphate buffer and incubated with a streptavidin/HRP-conjugated secondary antibody (Biocare Medical, Concord, CA, USA) for 30 min. Immunoreactivity to the various proteins was visualized with a colorimetric-based detection kit following the protocol provided by the manufacturer (TrekAvidin-HRP Label + Kit from Biocare Medical, Dako, USA). Sections were counter-stained with hematoxylin. Known positive controls and negative controls were included in each set of samples. Planimetry microscopy (Nikon E200 LED, Morphology Department/UFRN) with a high-power objective (40×) was utilised to score the intensity of cell immunostaining: 1 = absence of positive cells; 2 = small number of positive cells or isolated cells; 3 = moderate number of positive cells; and 4 = large number of positive cells. Labelling intensity was evaluated by two previously trained examiners in a double-blind fashion. Three tissue sections per animal (six animals per group) were evaluated.

Immunofluorescence microscopy

Three tissue sections from each animal (six animals per group) were deparaffinized in xylene and washed in a series of concentrations of ethanol and PBS. Antigen retrieval was performed by placing the sections in a 10 mM sodium

citrate with 0.05% Tween 20 for 40 min at 95°C. Autofluorescence background noise was reduced by incubating the sections in 0.1% Sudan black in 70% alcohol for 40 min at room temperature (RT). The sections were incubated overnight with rabbit anti-IL-1β, TNF- β and MIF primary antibody (1:200, 1:400 e 1:400 Abcam, EUA and Santa Cruz Biotechnology, USA, respectively), in blocking solution/1% normal goat serum; Abcam, USA and Santa Cruz Biotechnology, USA, respectively) at 4°C, washed three times in PBS/0.2% triton X-100 for 5 min and incubated with Alexa Fluor 488- conjugated goat anti-rabbit secondary antibody (1:500 in BSA 1%) and DAPI nuclear counterstain (Sigma, USA). Finally, the sections were mounted with Vectashield medium. Fluorescent images were obtained as described by (de Araújo et al. 2016).

Western blot analyses expression

The liver segments were homogenized in RIPA lysis buffer (25 mM Tris-HCL, pH 7.6; 150 mM NaCl; 5 mM EDTA; 1% NP40; 1% triton X-100; 1% sodium deoxycholate; 0.1% SDS) and protease inhibitor (1 µL inhibitor: 100 µL RIPA). For protein extraction, liver samples were centrifuged (17 min, 4°C, 13000 rpm) and the supernatant was collected. Protein concentrations were determined through the acid assay (Thermo Fisher Scientific) according to the manufacturer`s protocol. SDS-polyacrylamide gel electrophoresis (10% or 8%) were performed using 50 µg of protein (previously prepared with sample buffer, BioRad and denatured at 95°C for 5 min). Then, the protein was transferred to a PVDF membrane (BioRad) for 2 h, blocked with 5% BSA for 1 h, incubated overnight with a primary antibody (mouse anti-β actin, sc-81178, 1:500, Santa Cruz Biotechnology; mouse anti-TGFβ- 1/2-sc80346, 1:200, Santa Cruz Biotechnology; mouse anti-ERK1/ERK2, 136200, 1:500, Invitrogen; Goat anti-Iba-1, ab107159, Abcam) and a secondary antibody (goat anti-rabbit, 656120, Invitrogen, 1:1000; goat anti-mouse IgG, 626520, Invitrogen, 1:500; or rabbit anti-goat, A16142, Invitrogen, 1:1000) for 1 h and 30 min. The membranes were incubated using the ECL system according to the manufacturer's instructions (BioRad) and the chemiluminescence signal was detected using the ChemiDocTM XRS system (BioRad). Densitometric quantification of bands was done through the software ImageJ (NIH, Bethesda, MD, USA).

Analysis of mRNA Expression

Total RNA was extracted from liver tissue with trizol reagent (Invitrogen Co. USA) and the SV Total RNA Isolation System (Promega, Madison, WI). First-strand cDNA was synthesized from 1 µg of total RNA with the ImProm-IITM Reverse Transcriptase System for RT-PCR (Promega) according to the manufacturer's protocol. Real-time quantitative PCR analyses of *GAPDH, PCI, PCIII, NF-Kβ, F4/80, AKT and PI3K* mRNAs were performed with SYBR Green Mix in the Applied Biosystems1 7500 FAST system (Applied Biosystems, Foster City, CA), according to a standard protocol with the following primers of table 1.

The reference gene for normalization was selected from an analysis of 18S (GenBank sequence NM_003286.2), ubiquitin C (UBC, NM_021009.4), β-actin (ACTB, NM_001101.3) and glyceraldehyde-3-phosphate dehydrogenase (GAPDH, NM_002046.3) genes. GAPDH was chosen as the reference gene because it did not present different amplification patterns (J. Zhang et al. 2014). As it is a constitutive gene for eukaryotes, the reference gene should not be modified in the disease.

All analyses were performed in a 7500 fast real-time PCR instrument (Applied Biosystems, CA, USA). The standard PCR conditions were as follow: 50°C for 2 min and 95°C for 10 min, followed by forty 30-s cycles at 94°C, a variable annealing primer temperature for 30s, and 72°C for 1 min. Reactions were carried in duplicate according to the TaqMan® fast universal PCR master mix (Applied Biosystems, Foster City, CA, USA) protocol in a total volume of 10 µL containing approximately 20 ng cDNA. Mean Ct values were used to calculate the relative expression levels of the target genes for the experimental groups, relative to those in the negative control group; expression data were normalized relative to the housekeeping gene GAPDH using the $2^{-\Delta\Delta Ct}$ formula.

Statistical analysis

The data is presented as means with their standard errors (SEM) or as medians. Analysis of variance (ANOVA) followed by Bonferroni test was used to in parametric tests. The Kruskal-Wallis and Dunn tests was used to compare medians for non-parametric tests (Graph Pad Prism 5.0 Software, La Jolla, CA, USA).

3. RESULTS

GNPs Biodistribution

After I.V. injection of GNPs, we can observe that the liver, kidneys and brain were the tissues where nanoparticles migration occurred most strongly, indicated in Figure 1A, by greater fluorescence intensity. In the figure 1B, shows the quantification of GNPs biodistribution in the main organs and that biodistribution of gold nanoparticles have a dose-dependent effect on the concentrations tested.

Intracellular localization of GNPs in macrophage

In vitro assays were performed in order to investigate how GNPs interact with the cells and whether they are internalized. We observed that GNPs appeared to be internalized by macrophages, likely in the form of agglomerates/aggregates as shown by the light microscopy (Fig. 2B and B.1), and in the spectrum of bright green by immunofluorescence microscopy (Fig. 2D.1). The absence of GNPs in control cells is represented by a lack of agglomerates (Fig. 2A) and absence of the bright green spectrum (Fig. 2C). When the distribution of the GNPs in the liver was evaluated, all mice exposed to GNPs accumulations of nanoparticles were traced in Kupffer cells (Fig. 2E-F), and Fig. 2.G. presents a Kupffer cell from the control group that did not receive GNPs. After analyzing the cells and the liver fragments, we observed that the GNPs appear to be primarily localized in the cytoplasm close to nuclei and excluded from them.

Effects of GNPs on MPO activity and on MDA and GSH levels

Livers from the ethanol + METH group had significantly greater myeloperoxidase (MPO) activity than livers harvested from the saline group ($P < 0.0001$), and this increase was attenuated in the ethanol + METH + GNP3 group that received treatment with 724.96 µg/kg GNPs (Figure 3A). This same group, in turn, significantly increased glutathione (GSH) levels ($P < 0.0001$) compared to positive control group (Figure 3C). The malonyldialdehyde (MDA) formation was significantly increased in the ethanol + METH group when compared to saline group ($P < 0.01$) and GNPs treated groups ($P < 0.01$, $P < 0.001$), as seen in Figure 3B.

Effect of GNPs treatment on inflammation

The combined treatment with ethanol and METH resulted in increased levels of IL-1β ($P < 0.001$) and TNF-α ($P < 0.001$) compared to saline group (Figure 3D-E). As noted, such combined treatment may induce side effects which could be reduced by GNPs treatment. Specifically, IL-1β and TNF-α levels in ethanol + METH + GNP3

group were lower than GNPs absence ($P < 0.05$ and $P < 0.001$, respectively).On the other hand, it can also be seen in Figure 3F, that the combined treatment of ethanol + METH + GNP3 was able to increase IL-10 levels ($P < 0.0001$) compared to ethanol + METH treatment alone.

Histopathological analysis

At the end of the treatments, the animals were euthanized and their livers excised for histopathological analysis. From then on, after 28 days of saline administration, no pathological changes were observed in the negative control group (Figure 4A-C), as indexed by a semiquantitative scoring system. However, as seen in Figure 4E-G, the rats liver from ethanol + METH group exhibited fat accumulation, lymphocytes and neutrophils infiltrate, and necrosis (thin arrows, circle with arrow heads and stars, respectively), resulting in a high pathology scores (Figure 4M). Additionally, the ethanol + METH group had significantly greater steatosis than the saline group. On the other hand, ethanol and METH-induced liver damage was reduced when associated with GNP3 treatment($P < 0.001$) compared to its respective control without GNPs (Figure 4G-K).The same effect, however, was not observed for ethanol + METH + GNP1/GNP2 treated groups (Figure 4I-J). Reduced inflammation was most clearly observed in the ethanol + METH + GNP3 treated group (Figure 4K), which exhibited decreased areas of steatosis, inflammatory infiltrate contains neutrophils and lymphocytes and reduced levels of necrosis relative to ethanol + METH group alone.

Negative control group livers had weak staining limited to centrilobular veins as shown in the Figure 4D. Liver sections from the positive control group exhibited marked portal fibrosis and staining between the hepatic cords (Figure 4H). The treated group with GNP3 had a significative ($P < 0.01$) fibrotic response as can be seen when comparing figures 4H, 4L and 4M. Morphometric quantification of Sirius red stained areas demonstrated an attenuation of the fibrotic process in the treated group compared to the positive control group. Figure 4M shows that treatment of the GNP3 group had an attenuation of the fibrotic process in the liver, according to the analysis of the tissue fractions with the application of the Ishak scores.

In addition, treatment with ethanol and METH combined with GNP3 was able to reduce the AST, ALT and hepatic triglycerides levels (Figure 5A-C) when compared

to the control groups. However, GNPs treatment modulated this ethanol and METH-induced hepatosteatosis and liver injury (Figure 05). After analyzing the data of ALT, AST, hepatic Triglycerides, pro-and anti-inflammatory cytokines, anatomopathological analysis, we concluded that among the 3 doses tested the GNP3 was the one that presented the best results, therefore the following tests as Immunohistochemistry, Immunofluorescence, Electronic Microscopy RT-PCR-*Real Time*, Western Blot, were performed only with the negative and postoperative control groups and the group treated with the best dose of GNPs (GNP3).

Immunohistochemistry and immunofluorescence

The histopathological analysis was followed with antibody labeling for transforming growth factor-beta (TGF-β), fibroblast growth factor (FGF), SOD-1 and GPX-1 observation. When compared to alone ethanol + METH exposure, the ethanol + METH + GNP3 group was able to reduce the TGF-β, FGF, SOD-1 ($P < 0.001$) and GPX-1 levels ($P < 0.01$), as observed in the Figure 6 and Figure 7. These changes were consistent with the normalization toward non-ethanol and METH exposure levels.

Evaluation of IL-1β, TNF-α and macrophage migration inhibitory factor (MIF) was carried out by labelling with antibodies conjugated with fluorescent agent. Cellular IL-1β, TNF-α and MIF labelling (green) were strong and diffuse in the ethanol + METH group (Figure 8B, 8E and 8H), poorly marked in the ethanol + METH + GNP3 group (Figure 8C, 8F and 8I), and absent in saline group (Figure 8A, 8D,and 8G). Densitometric analysis confirmed that there were significantly increased IL-1β, TNF-α and MIF immunoreactivities in the ethanol +METH group, relative to the saline group, and lower immunoreactivity in the ethanol + METH + GNP3 group (Figure 8J,8K, and 8L).

GNPs treatment decreased NF-κB, F480, AKT, PI3K, PCI and PCIII mRNA expression

For all evaluated genes the relative mRNA expression was decreased when the groups were treated with ethanol + METH + GNP3 in relation to their respective control without the GNP3 ($P < 0.0001$ or $P < 0.001$), as observed in Figure 9A-F.

IBA-1, ERK1/ERK2 and TGF-β expression

The final product of ionized calcium-binding adaptor molecule 1 (IBA-1), ERK1/ERK2 and TGF-β genes expression into rats liver, exposed to ethanol + METH, was evaluated by western blot as show Figure 9G. Increased expression of IBA-1, ERK1 and TGF-β and decreased expression of ERK2in the ethanol + METH + GNP3 group were observed. The final product of IBA, ERK1/ERK2 and TGF-β genes expression into rats' liver, exposed to ethanol + METH, was evaluated by western blot as show Figure 9G. Increased expression of IBA-1, ERK1 and TGF-β and decreased expression of ERK2 in the ethanol + METH + GNP3 group were observed. No overexpression of IBA-1, ERK1 and TGF-β, already in the positive control group we observed intense marking intense labeling of the analyzed proteins.

4. Discussion

This study is the first into examine the anti-inflammatory, anti-oxidant and anti-fibrotic activity of GNPs in a rat model after ethanol and METH-induced liver injury through an analysis of markers of the inflammatory, oxidant and fibrotic processes. This was perfectly evidenced by a significant increase in several biochemical parameters such as oxidative stress, biomarkers of inflammation, severe fat accumulation, necrosis and accumulation of collagen type I and III around the hepatic triad which resulting in an strong steatosis beyond elevated neutrophil, MPO, and pro-inflammatory cytokine levels were also found all these changes were well evidence in the positive control groups.

When comparing the results obtained in this research with the results obtained previously (de Araújo et al. 2017), we have noticed that the dose used and the size of the GNPs are a key factor for effectiveness in the treatment with GNPs. Previously our group, observed that the highest GNPs dose (1500 μg/kg) generated 49% of reduction in leukocyte migration, which attested the activation of a cellular anti-inflammatory response, while the groups received GNPs showed decreases levels in the pro-inflammatory cytokine IL-1β (700 and 1500 μg/kg, $P < 0.05$) and TNF-α (700, 1000 and 1500 μg/kg, $P < 0.001$) compared to positive control group(de Araújo et al. 2017). Other studies also showed this relation of importance of the size of GNP and increased expression of proinflamatory cytokines (Khan et al. 2013; Ibrahim et al. 2018).

From the biodistribution tests, we have shown that after 48 h GNPs migrated mainly to the spleen, kidney and liver, reaching $2x10^5$, $5x10^5$ and $6x10^5$ ID/g, respectively, corroborating with the results seen earlier(de Araújo et al. 2017)and evidencing that after administration these GNPs migrate to the nucleus of Kupffer cells in the liver.

Studies have shown that the extent of cerebral uptake of anionic nanoparticles is higher than cationic and neutral GNPs(Noor, Fahmy, and Mourad 2016; Goodman et al. 2004). In this way, the surface of the NPs should be considered in the neurotoxicity profile and in the distribution, since neutral charges present irrelevant neurotoxicity (Masserini 2013). Not all types of nanoparticles are feasible for use in a strategy whose objective is to cross the blood-brain barrier (BBB). Surface characteristics vary depending on the nanomaterials used and it was found that neutral nanoparticles and low concentration anionic effects have no effect on this barrier (De Jong and Borm 2008).

In previous studies, we observed that results indicated that GNPs at the low concentrations below to 2 ppm did not show any toxicity, but at the higher concentrations, significant changes were observed in the organ (de Araújo et al. 2017; X. D. Zhang et al. 2010; Mironava et al. 2010). However, this accumulation of GNPs in the liver did not cause any morphological changes in this organ(de Araújo et al. 2017). GNPs (13 nm in diameter) after 28 days existed with the amount of 1.5% - 9.2% in the kidneys, while the amount is negligible in the urine (Yang et al. 2007). Extreme changes in the histopathology of lung and liver tissues caused by spherical GNPs with 5-10 nm size in 5 (5000 µg/kg), 10 (10.000 µg/kg), and 100 (100.0000 µg/kg) ppm treatment groups, been the pathological changes (lung and liver tissue) in treatment group (Au 100 ppm) more intense compared to the other groups (Abdelhalim and Jarrar 2011). However, in this work was used 0,724 ppm GNPs in the treatment groups. However, in our work was used dose of 0,724 (724 µg/kg) ppm GNPs in the treatment groups in the groups that presented the best results.

Some works have showed a non-immunogenic character of the GNPs or have even proven their anti-inflammatory effect, consisting of the reactive oxygen and nitrite species inhibition as well as pro-inflammatory cytokines in macrophages (Kurniawan et al. 2017; Q. Zhang et al. 2011). *In vivo* experiments also conducted on

several animal models of inflammatory conditions have confirmed the anti-inflammatory and antioxidant properties of the GNPs, manifested by a decrease in the levels of pro-inflammatory cytokines (IL-1β,TNF-α) and oxidative tissue damage markers (de Araújo et al. 2017; Tsai et al. 2012; Dohnert et al. 2012; Sumbayev et al. 2013).

Oxidative stress is known to play a crucial role in METH-induced toxicity in the brain and other tissues, as evidenced by previous studies. However, a comparison of oxidative effects of MET in different organs has not been sufficiently studied previously (Tokunaga et al. 2006). It has been suggested that the hepatic catalase level is negatively associated with the severity of alcoholic liver injury(de Araújo et al. 2016; Powell et al. 2010) and that SODs scavenge hydroxyl peroxides generated in the cytosol and mitochondria, thereby terminating autoxidation.

Gold nanoparticles can increase the anti-oxidant defense enzymes and creating a sustained such as GSH, SOD, Catalase and GPx in diabetic mice to normal, by inhibition of lipid peroxidation and ROS generation (Barathmanikanth et al. 2010). In this work, ethanol associated to METH imbalanced the hepatocellular antioxidant system, inflammatory cytokines and liberated the free radicals (Khan et al. 2012), as evidenced by the decrease in GSH level and the increased levels of MDA and MPO in hepatic tissue. GNPs724.96 µg/kg, however, increased hepatic GSH level and SOD-1 and GPX-1 expression, as well as decreased the MDA and MPO levels. Other studies in model of acute peritonitis study suggest that gold NPs of 10 nm diameter produce significant lipid peroxidation in rat liver however lungs and heart do not show any oxidative stress(Khan et al. 2012). That probably do not apply to our GNPs because they are smaller in size.

Ethanol pre-treatment was also able to exacerbate METH-induced hepatotoxicity, which could be ascertained by the significant increase of plasma transaminases activities, (hepatic lesion biomarkers), when animals were exposed to ethanol and METH. The increase in AST, ALT and triglycerides levels were already described for both compounds in humans (Ellis et al. 1996; Yue et al. 2006) and rats (Beitia et al. 2000; Montet et al. 2002). Increased prostaglandin E_2 (PGE_2) causes triglycerides accumulation in hepatocytes, and therefore, a state of steatosis(Bautista 2002). This hepatotoxic effect was also confirmed by the decrease in liver weight

when METH was administered to ethanol pre-exposed rats and by histological analysis of liver sections by light and electron microscopy, which gives further evidences that the concomitant exposure to METH and ethanol results in a marked aggravation of the hepatotoxic effects such as fat accumulation, lymphocytes and neutrophils infiltrate, necrosis and fibrosis (de Araújo et al. 2016). GNPs724.96 µg/kg, in turn, reduced all these histopathologic features.

Hepatocyte apoptosis causes recruitment of inflammatory cells to damaged liver and release of pro-fibrogenic cytokines (TGF-β1, IL-6, IL-1β, TNF-α) (Potter and Mezey 2007; Seki et al. 2007). IL-10 is a potent anti-inflammatory molecule that has been shown to inhibit TNF-α and IL-1 cytokines production and to suppress NF-κB activation (Mandal, Pritchard, and Nagy 2010). IL-10 reduces nitric oxide and reactive oxygen intermediates macrophage production, and also reduces adhesion molecules and chemokines expression (Gao 2012). Bone marrow (BM) derived and liver resident macrophages (Kupffer cells, KC) produce TGF-β1 in the fibrotic liver (Potter and Mezey 2007). TGF-β1 is a critical for activation of fibrogenic myofibroblasts, which in response to injury up-regulate α-smooth muscle actin (α-SMA) and secrete extracellular matrix proteins, mostly collagen Type I (Col) (Seki et al. 2007).

Hepatic stellate cells (HSCs) are the major source of fibrogenic myofibroblast in liver injury. There is an overwhelming evidence that activated HSCs are the major producers of the fibrotic matrix and that HSC apoptosis is the primary mechanism of regression of liver fibrosis (Kweon et al. 2003). Inflammation is the main characteristic in liver fibrosis and KCs are considered to be the primary source of inflammatory cytokines (Nieto 2006). In this study, we show that IL-1β, TNF-α levels and PCI and PCIII mRNA expression were increased while IL-10 cytokine was decreased in ethanol + METH group alone. On the other hand, inverted results were found in the 724.96µg/kg GNPs. Besides, our findings show that GNPs724.96µg/kg treatment inhibited NF-κB mRNA expression significantly.

The stimulatory effect of macrophage migration inhibitory factor(MIF) is, at least partly, dependent on IL-1β and IL-23 production, and involves the signaling pathways of MAP kinase (MAPK) (Gordon, Plüddemann, and Martinez Estrada 2014). The activated PI3-K participate in regulation of HSC migration, proliferation, collagen secretion and adhesion (Friedman 2000) besides being involved in

regulating a number of cellular responses, such as cell growth, survival and migration. The AKT is downstream of PI3-K and activation of AKT is associated with HSC proliferation and α1 (I) collagen transcription and translation (Reif et al. 2003). In the liver, macrophage-associated PI3K activation promotes cytokine production and subsequent hepatocyte proliferation early following partial hepatectomy (Jackson et al. 2008). Hepatocyte-associated PI3K regulates growth following a reduction in the liver volume, a process involving AKT activation. The activated PI3K/AKT was found to participate in regulation of HSC migration, proliferation, collagen secretion, and adhesion (Reif et al. 2003; Aslan, Lakowicz, and Geddes 2004). In the present work, GNPs 724.96 µg/kg inhibited macrophage-specific adhesion (F4/80), PI3K and AKT mRNA expression.

Compared with GNPs, negatively charged were retained longer in liver and spleen, presumably due to internalization by Kupffer cells and macrophages causing the formation of oxygen reaction species (Wang et al. 2016). GNPs appear to a type of be one of the promising treatment for hepatic injury, when the GNPs enter in the bloodstream, they are trapped by the Kupffer cells in the liver, or if smaller than about 4–6 nm partially be filtrated into the preurine (Sadauskas et al. 2007; Sereemaspun, Rojanathanes, and Wiwanitkit 2008) where the nanoparticle retention in the liver and spleen is low suggesting elimination through the kidneys. This mechanism seems to be very efficient and capable of protecting the rest of the organism from the nanoparticles (Sadauskas et al. 2007).

In our study, we showed that 724.96 µg/kg GNPs down-regulated the activity of Kupffer cells and hepatic stellate cells affecting the profile of their pro-inflammatory cytokines, oxidative stress and fibrosis through modulation of signaling pathways AKT/PI3K and MAPK.

Acknowledgments:

The authors are grateful to the Brain Institute (Federal University of Rio Grande do Norte) and the Leiden University Medical Center for their contributions to the present study. We acknowledge support by postdoctoral fellowship from the Raimundo Fernandes de Araujo Junior by CAPES 88881.119850/2016-01 and the

European Commission where RFde A, ABC and LJC have received funding from a MSCA-ITN-2015-ETN Action grant (proposal number: 675743; project: ISPIC).

Conflict of interest statement:

The authors declare no conflicts of interest.

5. Reference

Abdelhalim, Mohamed Anwar K, and Bashir M Jarrar. 2011. “Gold Nanoparticles Induced Cloudy Swelling to Hydropic Degeneration, Cytoplasmic Hyaline Vacuolation, Polymorphism, Binucleation, Karyopyknosis, Karyolysis, Karyorrhexis and Necrosis in the Liver.” *Lipids in Health and Disease* 10 (1): 166. https://doi.org/10.1186/1476-511X-10-166.

Almalki, Atiah H, Sujan C Das, Fahad S Alshehri, Yusuf S Althobaiti, and Youssef Sari. 2018. “Effects of Sequential Ethanol Exposure and Repeated High-Dose Methamphetamine on Striatal and Hippocampal Dopamine, Serotonin and Glutamate Tissue Content in Wistar Rats.” *Neuroscience Letters* 665 (Supplement C): 61–66. https://doi.org/https://doi.org/10.1016/j.neulet.2017.11.043.

Araújo, Raimundo Fernandes de, Aurigena Antunes de Araújo, Jonas Bispo Pessoa, Franscisco Paulo Freire Neto, Gisele Ribeiro da Silva, Ana Luiza C.S. Leitão Oliveira, Thaís Gomes de Carvalho, et al. 2017. “Anti-Inflammatory, Analgesic and Anti-Tumor Properties of Gold Nanoparticles.” *Pharmacological Reports* 69 (1): 119–29. https://doi.org/10.1016/j.pharep.2016.09.017.

Araújo, Raimundo Fernandes De, Vinícius Barreto Garcia, Renata Ferreira De Carvalho Leitão, Gerly Anne De Castro Brito, Emilio De Castro Miguel, Paulo Marcos Matta Guedes, and Aurigena Antunes De Araújo. 2016. “Carvedilol Improves Inflammatory Response, Oxidative Stress and Fibrosis in the Alcohol-Induced Liver Injury in Rats by Regulating Kuppfer Cells and Hepatic Stellate Cells.” *PLoS ONE* 11 (2). https://doi.org/10.1371/journal.pone.0148868.

Aslan, Kadir, Joseph R. Lakowicz, and Chris D. Geddes. 2004. “Nanogold-Plasmon-Resonance-Based Glucose Sensing.” *Analytical Biochemistry* 330 (1): 145–55. https://doi.org/10.1016/j.ab.2004.03.032.

Barathmanikanth, Selvaraj, Kalimuthu Kalishwaralal, Muthuirulappan Sriram, Sureshbabu Ram Kumar Pandian, Hyung-Seop Youn, Soohyun Eom, and Sangiliyandi Gurunathan. 2010. “Anti-Oxidant Effect of Gold Nanoparticles Restrains Hyperglycemic Conditions in Diabetic Mice.” *Journal of Nanobiotechnology* 8: 16. https://doi.org/10.1186/1477-3155-8-16.

Bartneck, M, K T Warzecha, and F Tacke. 2014. “Therapeutic Targeting of Liver Inflammation and Fibrosis by Nanomedicine.” *Hepatobiliary Surg Nutr* 3 (6): 364–76. https://doi.org/10.3978/j.issn.2304-3881.2014.11.02.

Bautista, A P. 2002. “Acute Ethanol Binge Followed by Withdrawal Regulates Production of Reactive Oxygen Species and Cytokine-Induced Neutrophil Chemoattractant and Liver Injury during Reperfusion after Hepatic Ischemia.” *Antioxid Redox Signal* 4 (5): 721–31. https://doi.org/10.1089/152308602760598864.

Beitia, G, a Cobreros, L Sainz, and E Cenarruzabeitia. 2000. “Ecstasy-Induced Toxicity in Rat Liver.” *Liver* 20 (1): 8–15. https://doi.org/10.1034/j.1600-0676.2000.020001008.x.

Chen, Ya-Ling, Li-Ju Chen, Ming-Jong Bair, Mei-Lan Yao, Hsiang-Chi Peng, Sien-Sing Yang, and Suh-Ching Yang. 2011. “Antioxidative Status of Patients with Alcoholic Liver Disease in Southeastern Taiwan.” *World Journal of Gastroenterology : WJG* 17 (8): 1063–70. https://doi.org/10.3748/wjg.v17.i8.1063.

De, Mrinmoy, and Vincent M Rotello. 2008. “Synthetic ‘chaperones’: Nanoparticle-Mediated Refolding of Thermally Denatured Proteins.” *Chemical Communications (Cambridge, England)*, no. 30: 3504–6. https://doi.org/10.1039/b805242e.

Dohnert, Marcelo B., Mirelli Venâncio, Jonathann C. Possato, Rodrigo C. Zeferino, Luciana H. Dohnert, Alexandra I. Zugno, Cláudio T. De Souza, Marcos M S Paula, and Thais F. Luciano. 2012. “Gold Nanoparticles and Diclofenac Diethylammonium Administered by Iontophoresis Reduce Inflammatory Cytokines Expression in Achilles Tendinitis.” *International Journal of Nanomedicine* 7: 1651–57. https://doi.org/10.2147/IJN.S25164.

Dykman, L A, and V A Bogatyrev. 2000. “Use of the Dot-Immunogold Assay for the Rapid Diagnosis of Acute Enteric Infections.” *FEMS Immunol. Med. Microbiol.* 27 (2): 135–37.

Ellis, A J, J A Wendon, B Portmann, and R Williams. 1996. “Acute Liver Damage and Ecstasy Ingestion.” *Gut* 38 (3): 454–58. https://doi.org/10.1136/gut.38.3.454.

Esterbauer, Hermann, and Kevin H. Cheeseman. 1990. “Determination of Aldehydic Lipid Peroxidation Products: Malonaldehyde and 4-Hydroxynonenal.” *Methods in Enzymology* 186 (C): 407–21. https://doi.org/10.1016/0076-6879(90)86134-H.

Friedman, S L. 2000. “Molecular Regulation of Hepatic Fibrosis, an Integrated Cellular Response to Tissue Injury.” *The Journal of Biological Chemistry* 275 (10): 2247–50. https://doi.org/10.1074/jbc.275.4.2247.

Fröhlich, Eleonore. 2012. “The Role of Surface Charge in Cellular Uptake and Cytotoxicity of Medical Nanoparticles.” *International Journal of Nanomedicine*. https://doi.org/10.2147/IJN.S36111.

Gao, Bin. 2012. “Hepatoprotective and Anti-Inflammatory Cytokines in Alcoholic Liver Disease.” *Journal of Gastroenterology and Hepatology* 27 Suppl 2: 89–93. https://doi.org/10.1111/j.1440-1746.2011.07003.x.

Gasparotto, Luiz H S, Amanda C. Garcia, Janaina F. Gomes, and Germano Tremiliosi-Filho. 2012. “Electrocatalytic Performance of Environmentally Friendly Synthesized Gold Nanoparticles towards the Borohydride Electro-Oxidation Reaction.” *Journal of Power Sources* 218: 73–78. https://doi.org/10.1016/j.jpowsour.2012.06.064.

Goodman, Catherine M., Catherine D. McCusker, Tuna Yilmaz, and Vincent M. Rotello. 2004. “Toxicity of Gold Nanoparticles Functionalized with Cationic and Anionic Side Chains.” *Bioconjugate Chemistry* 15 (4): 897–900. https://doi.org/10.1021/bc049951i.

Gordon, Siamon, Annette Plüddemann, and Fernando Martinez Estrada. 2014. “Macrophage Heterogeneity in Tissues: Phenotypic Diversity and Functions.”

Immunological Reviews 262 (1): 36–55. https://doi.org/10.1111/imr.12223.

Gunes, Y, L Y Y, H A Gumrukcuoglu, and M Tuncer. 2010. “Role of Echocardiography in the Evaluation of Atrial Function and Diseases.” *Minerva Cardioangiologica* 58 (3): 379–97. http://www.ncbi.nlm.nih.gov/pubmed/20485242.

Guo, Rui, Li Zhong, and Jun Ren. 2009. “Overexpression of Aldehyde Dehydrogenase-2 Attenuates Chronic Alcohol Exposure-Induced Apoptosis, Change in Akt and Pim Signalling in Liver.” *Clinical and Experimental Pharmacology and Physiology* 36 (5–6): 463–68. https://doi.org/10.1111/j.1440-1681.2009.05152.x.

Halpin, Laura E., William T. Gunning, and Bryan K. Yamamoto. 2013. “Methamphetamine Causes Acute Hyperthermia-Dependent Liver Damage.” *Pharmacology Research and Perspectives* 1 (1). https://doi.org/10.1002/prp2.8.

He, Wei, Zhi Huang Cheng, Fang Li Yuan, Ping Xie Jian, Ge Yang Rong, Fu Zhou Pei, and Jian Wang. 2008. “One-Step Label-Free Optical Genosensing System for Sequence-Specific DNA Related to the Human Immunodeficiency Virus Based on the Measurements of Light Scattering Signals of Gold Nanorods.” *Analytical Chemistry* 80 (22): 8424–30. https://doi.org/10.1021/ac801005d.

Hirsch, L R, R J Stafford, J A Bankson, S R Sershen, B Rivera, R E Price, J D Hazle, N J Halas, and J L West. 2003. “Nanoshell-Mediated near-Infrared Thermal Therapy of Tumors under Magnetic Resonance Guidance.” *Proceedings of the National Academy of Sciences of the United States of America* 100 (23): 13549–54. https://doi.org/10.1073/pnas.2232479100.

Ibrahim, Khalid Elfaki, Amel Omer Bakhiet, Maaweya Elaeed Awadalla, and Haseeb Ahmad Khan. 2018. “A Priming Dose Protects against Gold Nanoparticles-Induced Proinflammatory Cytokines mRNA Expression in Mice.” *Nanomedicine* 13 (3): 313–23. https://doi.org/10.2217/nnm-2017-0332.

Ikegami, Aiko, Christopher M. Olsen, Sheila M. Fleming, Erik E. Guerra, Michael A. Bittner, Jeremy Wagner, and Christine L. Duvauchelle. 2002. “Intravenous Ethanol/cocaine Self-Administration Initiates High Intake of Intravenous Ethanol

Alone.” *Pharmacology Biochemistry and Behavior* 72 (4): 787–94. https://doi.org/10.1016/S0091-3057(02)00738-4.

Ishak, Kamal, Amelia Baptista, Leonardo Bianchi, Francesco Callea, Jan De Groote, Fred Gudat, Helmut Denk, et al. 1995. “Histological Grading and Staging of Chronic Hepatitis.” *Journal of Hepatology* 22 (6): 696–99. https://doi.org/10.1016/0168-8278(95)80226-6.

Jackson, Lindsey N, Shawn D Larson, Scott R Silva, Piotr G Rychahou, L Andy Chen, Suimin Qiu, Srinivasan Rajaraman, et al. 2008. “PI3K / Akt Activation Is Critical for Early Hepatic Regeneration after Partial Hepatectomy” 536: 1401–10. https://doi.org/10.1152/ajpgi.00062.2008.

Jong, Wim H De, and Paul J a Borm. 2008. “Drug Delivery and Nanoparticles:applications and Hazards.” *International Journal of Nanomedicine* 3 (2): 133–49. https://doi.org/10.2147/IJN.S596.

Kang, N J, K M Lee, J H Kim, B K Lee, J Y Kwon, K W Lee, and H J Lee. 2008. “Inhibition of Gap Junctional Intercellular Communication by the Green Tea Polyphenol (-)-Epigallocatechin Gallate in Normal Rat Liver Epithelial Cells.” *J Agric Food Chem* 56 (21): 10422–27. http://www.ncbi.nlm.nih.gov/entrez/query.fcgi?cmd=Retrieve&db=PubMed&dopt=Citation&list_uids=18828601.

Kedia, Satish, Marie A Sell, and George Relyea. 2007. “Mono- versus Polydrug Abuse Patterns among Publicly Funded Clients.” *Substance Abuse Treatment, Prevention, and Policy* 2: 33. https://doi.org/10.1186/1747-597X-2-33.

Khan, Haseeb A., Mohamed Anwar K Abdelhalim, Mohammed S. Al-Ayed, and Abdullah S. Alhomida. 2012. “Effect of Gold Nanoparticles on Glutathione and Malondialdehyde Levels in Liver, Lung and Heart of Rats.” *Saudi Journal of Biological Sciences* 19 (4): 461–64. https://doi.org/10.1016/j.sjbs.2012.06.005.

Khan, Haseeb A., Mohamed Anwar K Abdelhalim, Abdullah S. Alhomida, and Mohammed S. Al-Ayed. 2013. “Effects of Naked Gold Nanoparticles on Proinflammatory Cytokines mRNA Expression in Rat Liver and Kidney.” *BioMed Research International* 2013. https://doi.org/10.1155/2013/590730.

Kirkpatrick, Matthew G., and Harriet De Wit. 2013. “In the Company of Others: Social Factors Alter Acute Alcohol Effects.” *Psychopharmacology* 230 (2): 215–26. https://doi.org/10.1007/s00213-013-3147-0.

Koriem, Khaled M M, and Rowan E. Soliman. 2014. “Chlorogenic and Caftaric Acids in Liver Toxicity and Oxidative Stress Induced by Methamphetamine.” *Journal of Toxicology* 2014. https://doi.org/10.1155/2014/583494.

Kurniawan, Alfin, Farrel Gunawan, Adi Tama Nugraha, Suryadi Ismadji, and Meng Jiy Wang. 2017. “Biocompatibility and Drug Release Behavior of Curcumin Conjugated Gold Nanoparticles from Aminosilane-Functionalized Electrospun poly(N-Vinyl-2-Pyrrolidone) Fibers.” *International Journal of Pharmaceutics* 516 (1–2): 158–69. https://doi.org/10.1016/j.ijpharm.2016.10.067.

Kweon, Young-Oh, Yong-Han Paik, Bernd Schnabl, Ting Qian, John J Lemasters, and David A Brenner. 2003. “Gliotoxin-Mediated Apoptosis of Activated Human Hepatic Stellate Cells.” *Journal of Hepatology* 39 (1): 38–46. https://doi.org/10.1016/S0168-8278(03)00178-8.

Loumaigne, Matthieu, Alain Richard, Julien Laverdant, Daniele Nutarelli, and Anne Débarre. 2010. “Ligand-Induced Anisotropy of the Two-Photon Luminescence of Spherical Gold Particles in Solution Unraveled at the Single Particle Level.” *Nano Letters* 10 (8): 2817–24. https://doi.org/10.1021/nl100737y.

MacParland, Sonya A., Kim M. Tsoi, Ben Ouyang, Xue Zhong Ma, Justin Manuel, Ali Fawaz, Mario A. Ostrowski, et al. 2017. “Phenotype Determines Nanoparticle Uptake by Human Macrophages from Liver and Blood.” *ACS Nano* 11 (3): 2428–43. https://doi.org/10.1021/acsnano.6b06245.

Mandal, Palash, Michele T. Pritchard, and Laura E. Nagy. 2010. “Anti-Inflammatory Pathways and Alcoholic Liver Disease: Role of an Adiponectin/interleukin-10/heme Oxygenase-1 Pathway.” *World Journal of Gastroenterology* 16 (11): 1330–36. https://doi.org/10.3748/wjg.v16.i11.1330.

Masserini, Massimo. 2013. “Nanoparticles for Brain Drug Delivery.” *ISRN Biochemistry* 2013: 1–18. https://doi.org/10.1155/2013/238428.

Mironava, Tatsiana, Michael Hadjiargyrou, Marcia Simon, Vladimir Jurukovski, and

Miriam H Rafailovich. 2010. “Gold Nanoparticles Cellular Toxicity and Recovery: Effect of Size, Concentration and Exposure Time.” *Nanotoxicology* 4 (1): 120–37. https://doi.org/10.3109/17435390903471463.

Montet, Anne-Marie, Laurence Oliva, Françoise Beaugé, and Jean-Claude Montet. 2002. “Bile Salts Modulate Chronic Ethanol-Induced Hepatotoxicity.” *Alcohol and Alcoholism (Oxford, Oxfordshire)* 37 (1): 25–29. http://www.ncbi.nlm.nih.gov/pubmed/11825853.

Nanji, Amin A., Charles L. Mendenhall, and Samuel W. French. 1989. “Beef Fat Prevents Alcoholic Liver Disease in the Rat.” *Alcoholism: Clinical and Experimental Research* 13 (1): 15–19. https://doi.org/10.1111/j.1530-0277.1989.tb00276.x.

Nieto, Natalia. 2006. “Oxidative-Stress and IL-6 Mediate the Fibrogenic Effects of Rodent Kupffer Cells on Stellate Cells.” *Hepatology* 44 (6): 1487–1501. https://doi.org/10.1002/hep.21427.

Noor, Neveen A, Heba M Fahmy, and Iman M Mourad. 2016. “Evaluation of the Potential Neurotoxicity of Gold Nanoparticles in the Different Rat Brain Regions” 4531 (December): 114–29.

Park, Ho Young, Hee Don Choi, Hyojin Eom, and Inwook Choi. 2013. “Enzymatic Modification Enhances the Protective Activity of Citrus Flavonoids against Alcohol-Induced Liver Disease.” *Food Chemistry* 139 (1–4): 231–40. https://doi.org/10.1016/j.foodchem.2013.01.044.

Pontes, Helena, Jos?? Alberto Duarte, Paula Guedes de Pinho, Maria Elisa Soares, Eduarda Fernandes, Ricardo Jorge Dinis-Oliveira, Carla Sousa, et al. 2008. “Chronic Exposure to Ethanol Exacerbates MDMA-Induced Hyperthermia and Exposes Liver to Severe MDMA-Induced Toxicity in CD1 Mice.” *Toxicology* 252 (1–3): 64–71. https://doi.org/10.1016/j.tox.2008.07.064.

Potter, James J., and Esteban Mezey. 2007. “Acetaldehyde Increases Endogenous Adiponectin and Fibrogenesis in Hepatic Stellate Cells but Exogenous Adiponectin Inhibits Fibrogenesis.” *Alcoholism: Clinical and Experimental Research* 31 (12): 2092–2100. https://doi.org/10.1111/j.1530-

0277.2007.00529.x.

Powell, Christine L., Blair U. Bradford, Christopher Patrick Craig, Masato Tsuchiya, Takeki Uehara, Thomas M. O'Connell, Igor P. Pogribny, et al. 2010. "Mechanism for Prevention of Alcohol-Induced Liver Injury by Dietary Methyl Donors." *Toxicological Sciences* 115 (1): 131–39. https://doi.org/10.1093/toxsci/kfq031.

Reif, Shimon, Alon Lang, Jeffery N. Lindquist, Yutaka Yata, Erwin Gäbele, Andrew Scanga, David A. Brenner, and Richard A. Rippe. 2003. "The Role of Focal Adhesion Kinase-Phosphatidylinositol 3-Kinase-Akt Signaling in Hepatic Stellate Cell Proliferation and Type I Collagen Expression." *Journal of Biological Chemistry* 278 (10): 8083–90. https://doi.org/10.1074/jbc.M212927200.

Sadauskas, Evaldas, Håkan Wallin, Meredin Stoltenberg, Ulla Vogel, Peter Doering, Agnete Larsen, and Gorm Danscher. 2007. "Kupffer Cells Are Central in the Removal of Nanoparticles from the Organism." *Part Fibre Toxicol* 4 (3): 10. https://doi.org/10.1186/1743-8977-4-10.

Safieh-Garabedian, B, S Poole, A Allchorne, J Winter, and C J Woolf. 1995. "Contribution of Interleukin-1 Beta to the Inflammation-Induced Increase in Nerve Growth Factor Levels and Inflammatory Hyperalgesia." *British Journal of Pharmacology* 115 (7): 1265–75. https://doi.org/0007-1188/95.

Sayette, Michael A., Kasey G. Creswell, John D. Dimoff, Catharine E. Fairbairn, Jeffrey F. Cohn, Bryan W. Heckman, Thomas R. Kirchner, John M. Levine, and Richard L. Moreland. 2012. "Alcohol and Group Formation: A Multimodal Investigation of the Effects of Alcohol on Emotion and Social Bonding." *Psychological Science* 23 (8): 869–78. https://doi.org/10.1177/0956797611435134.

Schaeublin, Nicole M, Laura K Braydich-Stolle, Amanda M Schrand, John M Miller, Jim Hutchison, John J Schlager, and Saber M Hussain. 2011. "Surface Charge of Gold Nanoparticles Mediates Mechanism of Toxicity." *Nanoscale* 3: 410–20. https://doi.org/10.1039/c0nr00478b.

Seki, Ekihiro, Samuele De Minicis, Christoph H Osterreicher, Johannes Kluwe,

Yosuke Osawa, David a Brenner, and Robert F Schwabe. 2007. “TLR4 Enhances TGF-Beta Signaling and Hepatic Fibrosis.” *Nature Medicine* 13 (11): 1324–32. https://doi.org/10.1038/nm1663.

Sereemaspun, Amornpun, Rojrit Rojanathanes, and Viroj Wiwanitkit. 2008. “Effect of Gold Nanoparticle on Renal Cell: An Implication for Exposure Risk.” *Renal Failure* 30 (3): 323–25. https://doi.org/10.1080/08860220701860914.

Son, Yong, Yong-Kwan Cheong, Nam-Ho Kim, Hun-Taeg Chung, Dae Gill Kang, and Hyun-Ock Pae. 2011. “Mitogen-Activated Protein Kinases and Reactive Oxygen Species: How Can ROS Activate MAPK Pathways?” *Journal of Signal Transduction* 2011: 792639. https://doi.org/10.1155/2011/792639.

Sumbayev, Vadim V., Inna M. Yasinska, Cesar Pascual Garcia, Douglas Gilliland, Gurprit S. Lall, Bernhard F. Gibbs, David R. Bonsall, Luca Varani, François Rossi, and Luigi Calzolai. 2013. “Gold Nanoparticles Downregulate Interleukin-1β-Induced pro-Inflammatory Responses.” *Small* 9 (3): 472–77. https://doi.org/10.1002/smll.201201528.

Tang, Yuhan, Yanyan Li, Haiyan Yu, Chao Gao, Liang Liu, Mingyou Xing, Liegang Liu, and Ping Yao. 2014. “Quercetin Attenuates Chronic Ethanol Hepatotoxicity: Implication Of ‘free’ iron Uptake and Release.” *Food and Chemical Toxicology* 67: 131–38. https://doi.org/10.1016/j.fct.2014.02.022.

Tilg, Herbert, and Alexander R Moschen. 2008. “Inflammatory Mechanisms in the Regulation of Insulin Resistance.” *Molecular Medicine (Cambridge, Mass.)* 14 (3–4): 222–31. https://doi.org/10.2119/2007-00119.Tilg.

Tokunaga, Itsuo, Shin-ichi Kubo, Akiko Ishigami, Takako Gotohda, and Osamu Kitamura. 2006. “Changes in Renal Function and Oxidative Damage in Methamphetamine-Treated Rat.” *Legal Medicine (Tokyo, Japan)* 8 (1): 16–21. https://doi.org/10.1016/j.legalmed.2005.07.003.

Tsai, Chiau-Yuang, Shiou-Ling Lu, Chia-Wen Hu, Chen-Sheng Yeh, Gwo-Bin Lee, and Huan-Yao Lei. 2012. “Size-Dependent Attenuation of TLR9 Signaling by Gold Nanoparticles in Macrophages.” *Journal of Immunology (Baltimore, Md. : 1950)* 188 (1): 68–76. https://doi.org/10.4049/jimmunol.1100344.

Wang, Jun Ying, Jie Chen, Jiang Yang, Hao Wang, Xiu Shen, Yuan Ming Sun, Meili Guo, and Xiao Dong Zhang. 2016. “Effects of Surface Charges of Gold Nanoclusters on Long-Term in Vivo Biodistribution, Toxicity, and Cancer Radiation Therapy.” *International Journal of Nanomedicine* 11: 3475–85. https://doi.org/10.2147/IJN.S106073.

Wells, Peter G., Shama Bhatia, Danielle M. Drake, and Lutfiya Miller-Pinsler. 2016. “Fetal Oxidative Stress Mechanisms of Neurodevelopmental Deficits and Exacerbation by Ethanol and Methamphetamine.” *Birth Defects Research Part C - Embryo Today: Reviews*. https://doi.org/10.1002/bdrc.21134.

Wen, Donghai, Xinzhong Huang, Min Zhang, Liying Zhang, Jing Chen, Yong Gu, and Chuan Ming Hao. 2013. “Resveratrol Attenuates Diabetic Nephropathy via Modulating Angiogenesis.” *PLoS ONE* 8 (12). https://doi.org/10.1371/journal.pone.0082336.

Winkler, Madeline C., Emilee M. Greager, Jacob Stafford, and Ryan K. Bachtell. 2016. “Methamphetamine Self-Administration Reduces Alcohol Consumption and Preference in Alcohol-Preferring P Rats.” *Addiction Biology*. https://doi.org/10.1111/adb.12476.

Yang, Raymond S H, Louis W. Chang, Jui Pin Wu, Ming Hsien Tsai, Hsiu Jen Wang, Yu Chun Kuo, Teng Kuang Yeh, Chung Shi Yang, and Pinpin Lin. 2007. “Persistent Tissue Kinetics and Redistribution of Nanoparticles, Quantum Dot 705, in Mice: ICP-MS Quantitative Assessment.” *Environmental Health Perspectives* 115 (9): 1339–43. https://doi.org/10.1289/ehp.10290.

Yin, Hu Quan, Youn Chul Kim, Young Suk Chung, Young Chul Kim, Young Kee Shin, and Byung Hoon Lee. 2009. “Honokiol Reverses Alcoholic Fatty Liver by Inhibiting the Maturation of Sterol Regulatory Element Binding Protein-1c and the Expression of Its Downstream Lipogenesis Genes.” *Toxicology and Applied Pharmacology* 236 (1): 124–30. https://doi.org/10.1016/j.taap.2008.12.030.

Yue, Min, Qun Ni, Chao Hui Yu, Ke Ming Ren, Wei Xing Chen, and You Ming Li. 2006. “Transient Elevation of Hepatic Enzymes in Volunteers after Intake of Alcohol.” *Hepatobiliary and Pancreatic Diseases International* 5 (1): 52–55.

Zendulka, O., M. Sabová, J. Juřica, M. MacHalíček, P. Švéda, M. Farková, and A. Šulcová. 2012. “The Effect of Methamphetamine on Biotransformation of Ethanol: Pilot Study.” *Acta Facultatis Pharmaceuticae Universitatis Comenianae* 59 (2): 63–71. https://doi.org/10.2478/v10219-012-0026-4.

Zhang, Juan, Hongju Tang, Yuqing Zhang, Ruyuan Deng, Li Shao, Yun Liu, Fengying Li, Xiao Wang, and Libin Zhou. 2014. “Identification of Suitable Reference Genes for Quantitative RT-PCR during 3T3-L1 Adipocyte Differentiation.” *International Journal of Molecular Medicine* 33 (5): 1209–18. https://doi.org/10.3892/ijmm.2014.1695.

Zhang, Qin, Victoria M Hitchins, Amanda M Schrand, Saber M Hussain, and Peter L Goering. 2011. “Uptake of Gold Nanoparticles in Murine Macrophage Cells without Cytotoxicity or Production of pro-Inflammatory Mediators.” *Nanotoxicology* 5 (September): 284–95. https://doi.org/10.3109/17435390.2010.512401.

Zhang, Xiao Dong, Hong Ying Wu, Di Wu, Yue Ying Wang, Jian Hui Chang, Zhi Bin Zhai, Ai Min Meng, Pei Xun Liu, Liang An Zhang, and Fei Yue Fan. 2010. “Toxicologic Effects of Gold Nanoparticles in Vivo by Different Administration Routes.” *International Journal of Nanomedicine* 5 (1): 771–81. https://doi.org/10.2147/IJN.S8428.

FIGURE CAPTIONS

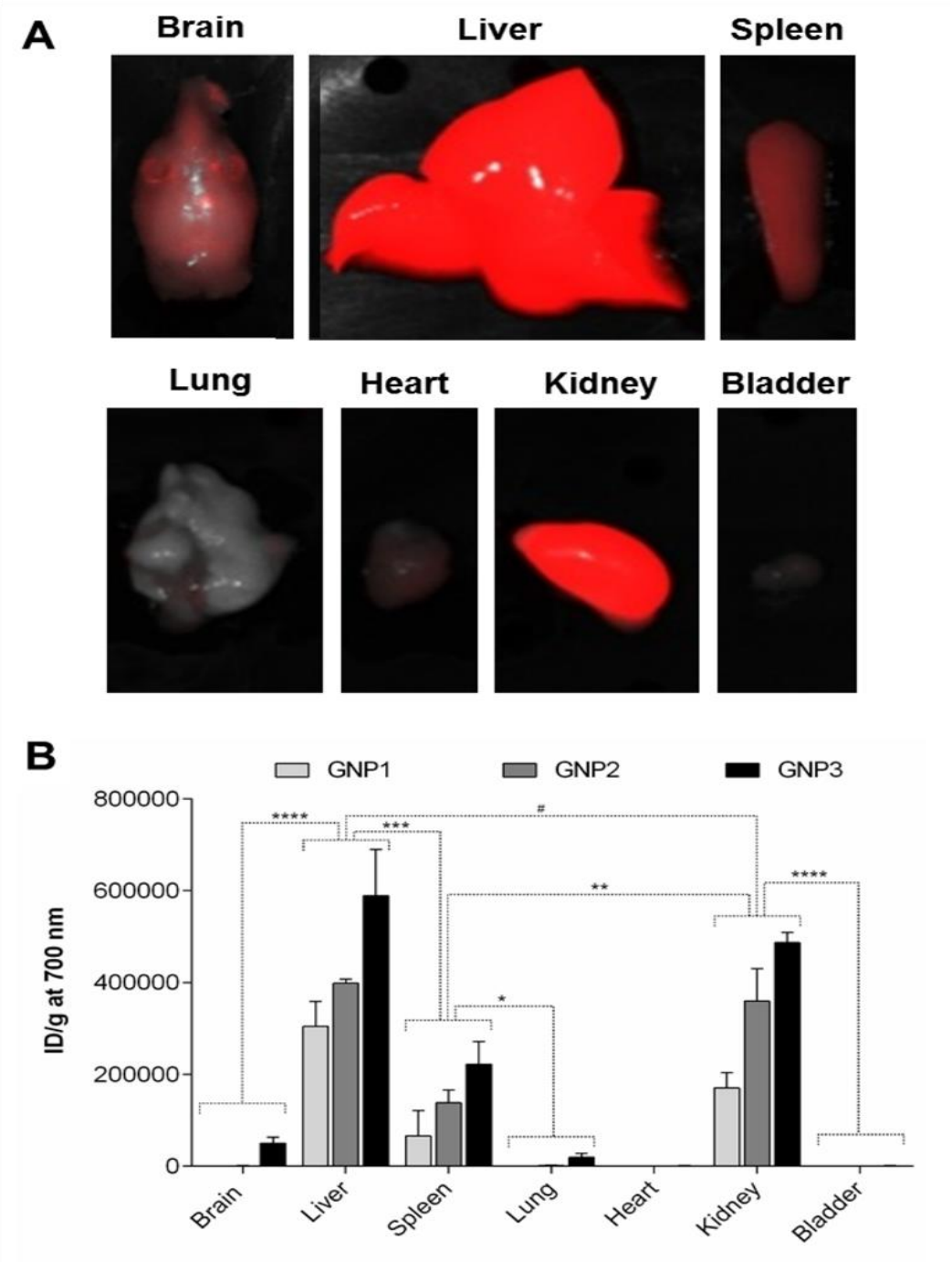

Figure 1.Tecidual biodistribution of GNPs. Main target organs of GNPs 48 h post **i.v**. injection of 14 µg/ml (A). Quantitative representation of GNPs distribution intensity at 700 nm in different organs (B). Quantification of GNPs biodistribution in the main organs.

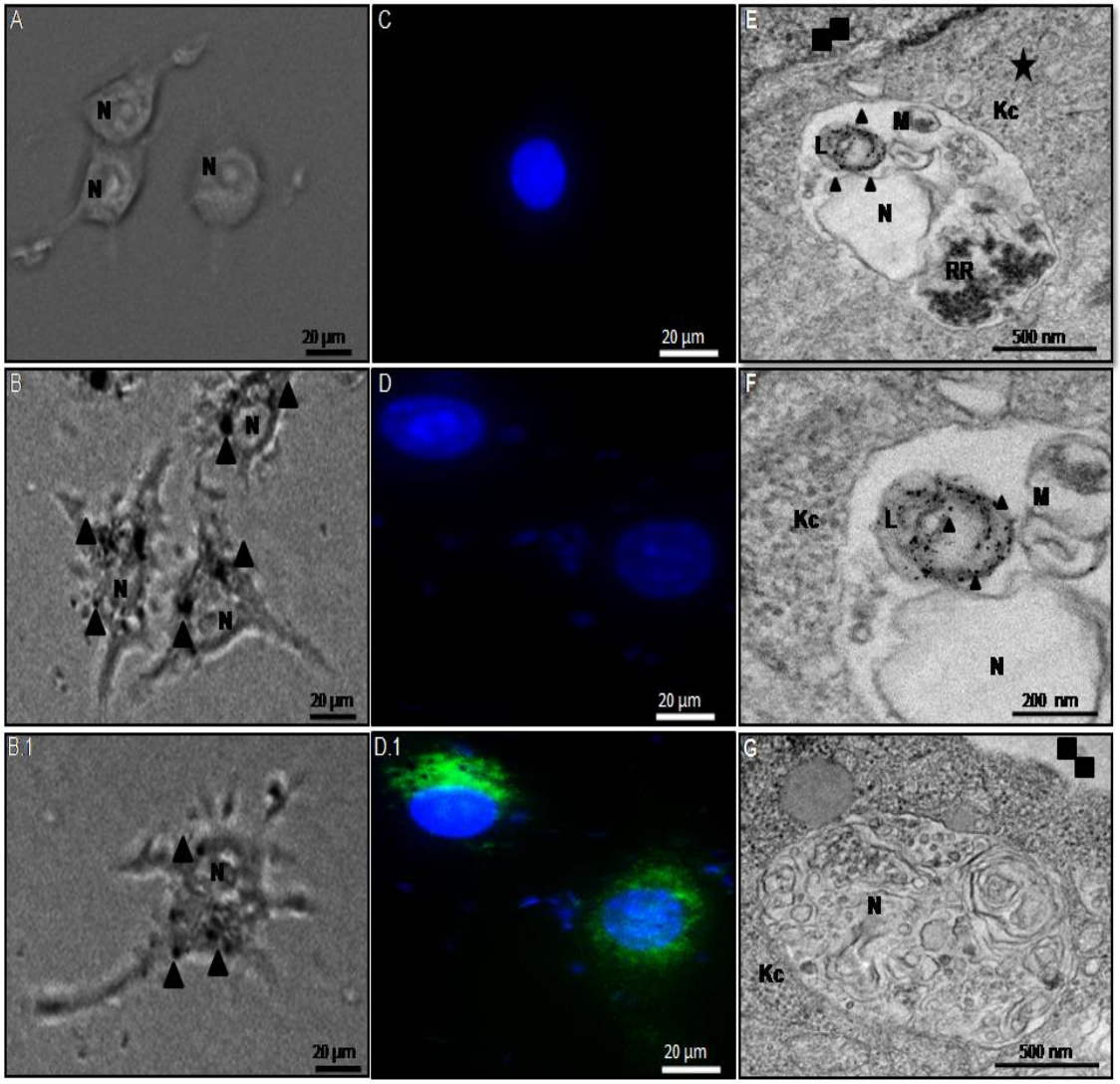

Figure 2. Intracellular localization of GNPs in macrophage. (B and D.1) and in Kupffer cells Lysossomos (E-G). Negative control, cell without GNPs (A and C). DAPI in blue (C and D) and GNPs in green (D.1). Kc: Kupffer cells; **N:** nucleus; Triangle: GNPs; **L**: lysosomes; Star: hepatocyte; Two square: Disse's spaces. Magnification: 400x. Uptake of nanoparticles was evaluated by Fluorescence microscopy (D1).

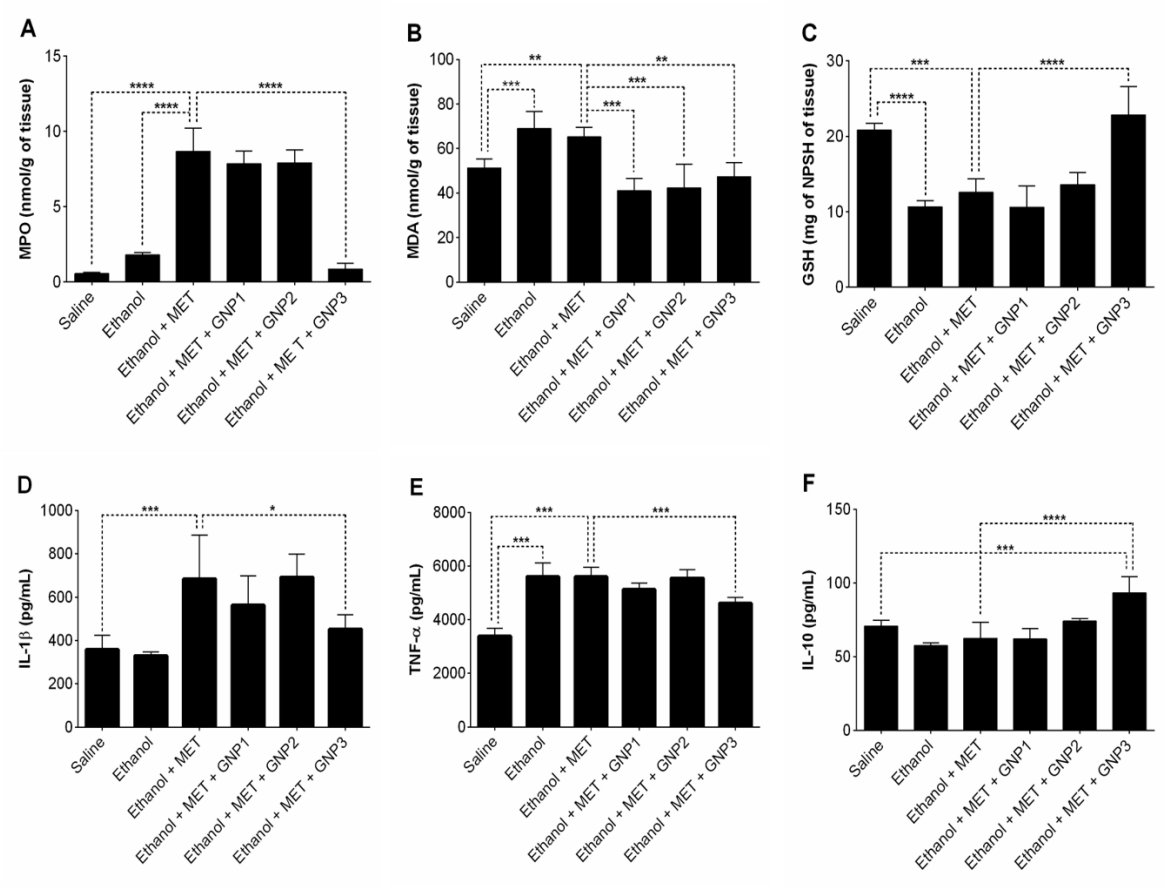

Figure 3. Modulation of the antioxidant activity and cytokine profile by GNPs. Myeloperoxidase activity (MPO) (A), malondialdehy deformation (MDA) (B), and reduced glutathione levels(GSH) (C).Cytokine analysis(D-F). METH, methamphetamine; GNP1, gold nanoparticles 181.48 µg/kg; GNP2, gold nanoparticles 362.48 µg/kg, GNP3, gold nanoparticles 724.96 µg/kg. *$p < 0.05$; **$p < 0.01$;***$p < 0.001$;****$p < 0.0001$.

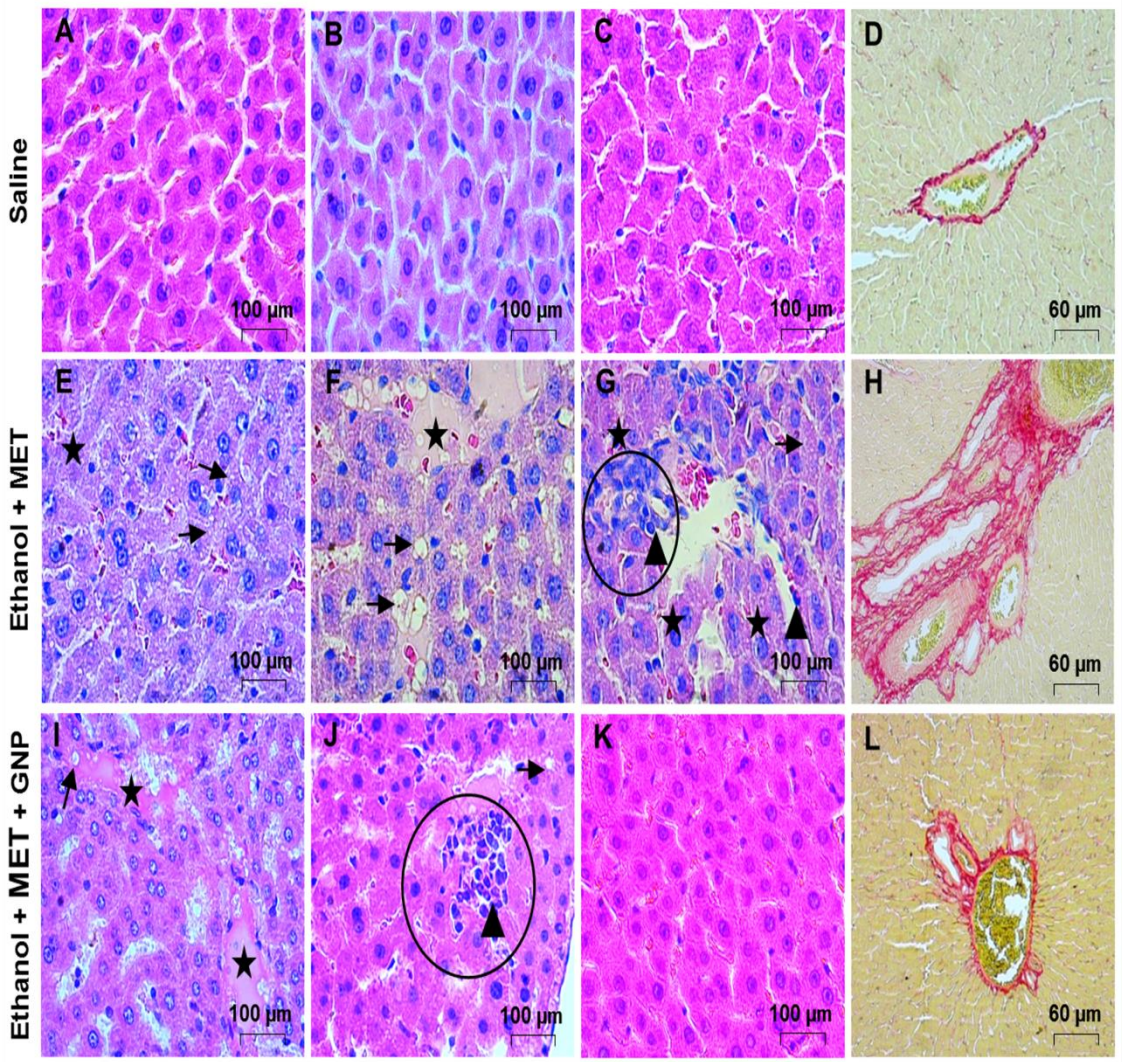
Saline
Ethanol + MET
Ethanol + MET + GNP
A
B
C
D
E
F
G
H
I
J
K
L
100 µm
60 µm
M
H&E
Picrosirius
Histopathological score
0
1
2
3
4
5
6
****
***
****
**
Saline
Ethanol + MET
Ethanol + MET + GNP1
Ethanol + MET + GNP2
Ethanol + MET + GNP3
Saline
Ethanol + MET
Ethanol + MET + GNP3

Figure 4. Histological analysis from hepatic parenchyma. Group treated with saline solution (A-D), alcohol 30% + methamphetamine (METH) (E-H) and groups treated with GNP1 191.24 µg/kg (I), GNP2 362.8 µg/kg (J), GNP3 724.96 µg/kg (K-L). Fibrosis analysis by Picrosirius staining (D, H and L).The area fraction of total fibrosis, including fibrosis in the portal tract area, in rats with GNP3 group induced liver injury in relation to the Ishak score. Graphical representation of the mean histopathological score from each treated group (M). Arrow, fatty changes within hepatocytes; arrow head, neutrophils; star: necrosis area; circle, lymphocytes and neutrophils infiltrate. Magnification 400x. *$p < 0.05$; **$p < 0.01$; ***$p < 0.001$; ****$p < 0.0001$.

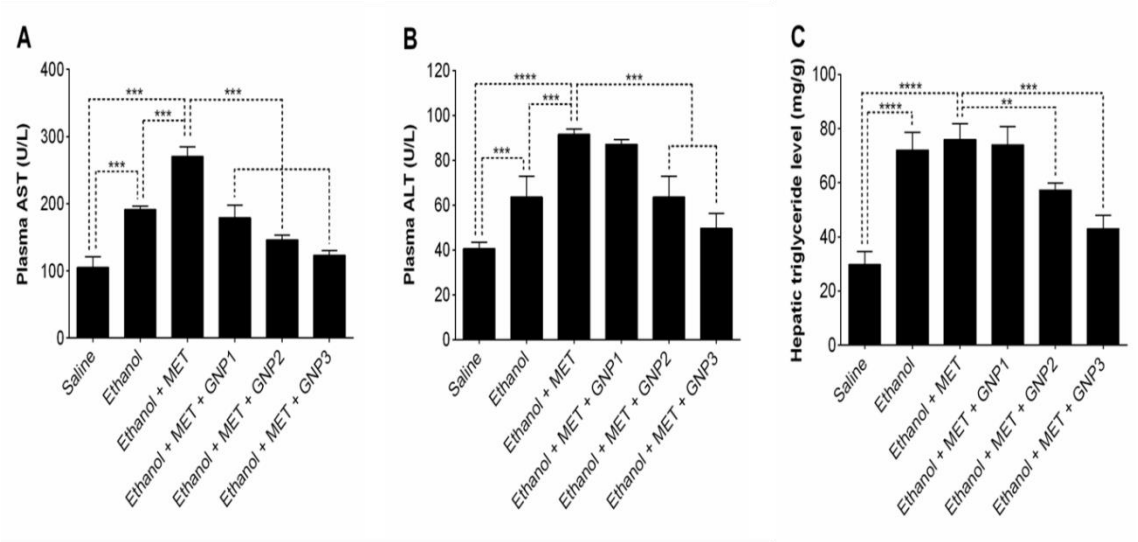

Figure 5. Biochemical assessments of liver function. (A) Aspartate aminotransferase (AST), (B) Alanine aminotransferase (ALT). (C) Triglyceride. METH, methamphetamine; GNP1, gold nanoparticles 181.48 µg/kg; GNP2, gold nanoparticles 362.48 µg/kg, GNP3, gold nanoparticles 724.96 µg/kg. $^{**}p < 0.01$; $^{***}p < 0.001$;$^{****}p < 0.0001$).

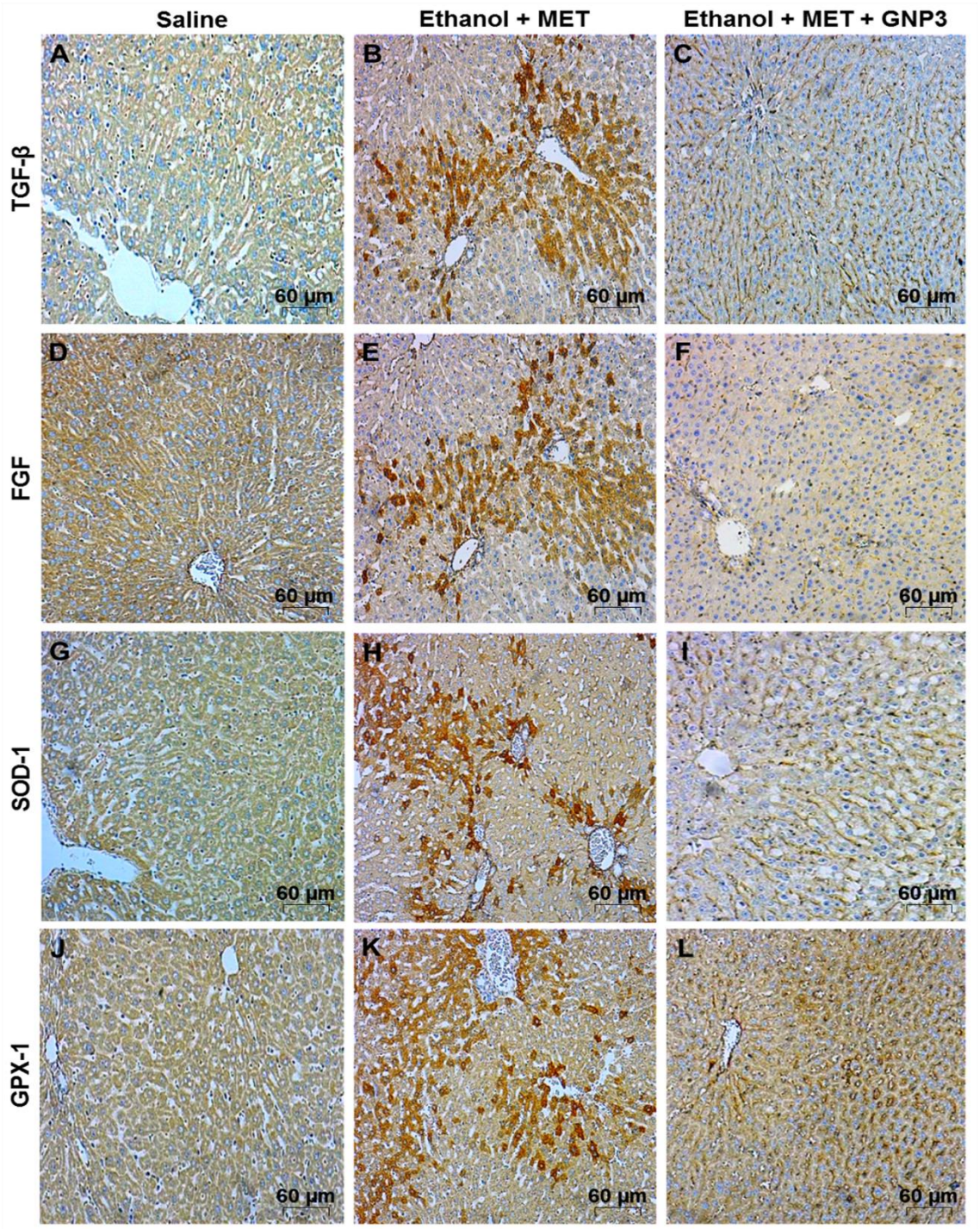

Figure 6. Immunohistochemical analysis from hepatic parenchyma. The saline (A, D, G, and J), alcohol + methamphetamine (B, E, H and K) and alcohol + methamphetamine + GNP 724.96 µg/kg (C, F, I and L) groups were labeled for evaluation of TGF-β(A-C) and FGF (D-F) growth factors, and for oxidative stress through SOD-1(G-I) and GPX-1 (J-L). METH, methamphetamine; GNP3, gold nanoparticles 724.96 µg/kg. Magnification 400x.

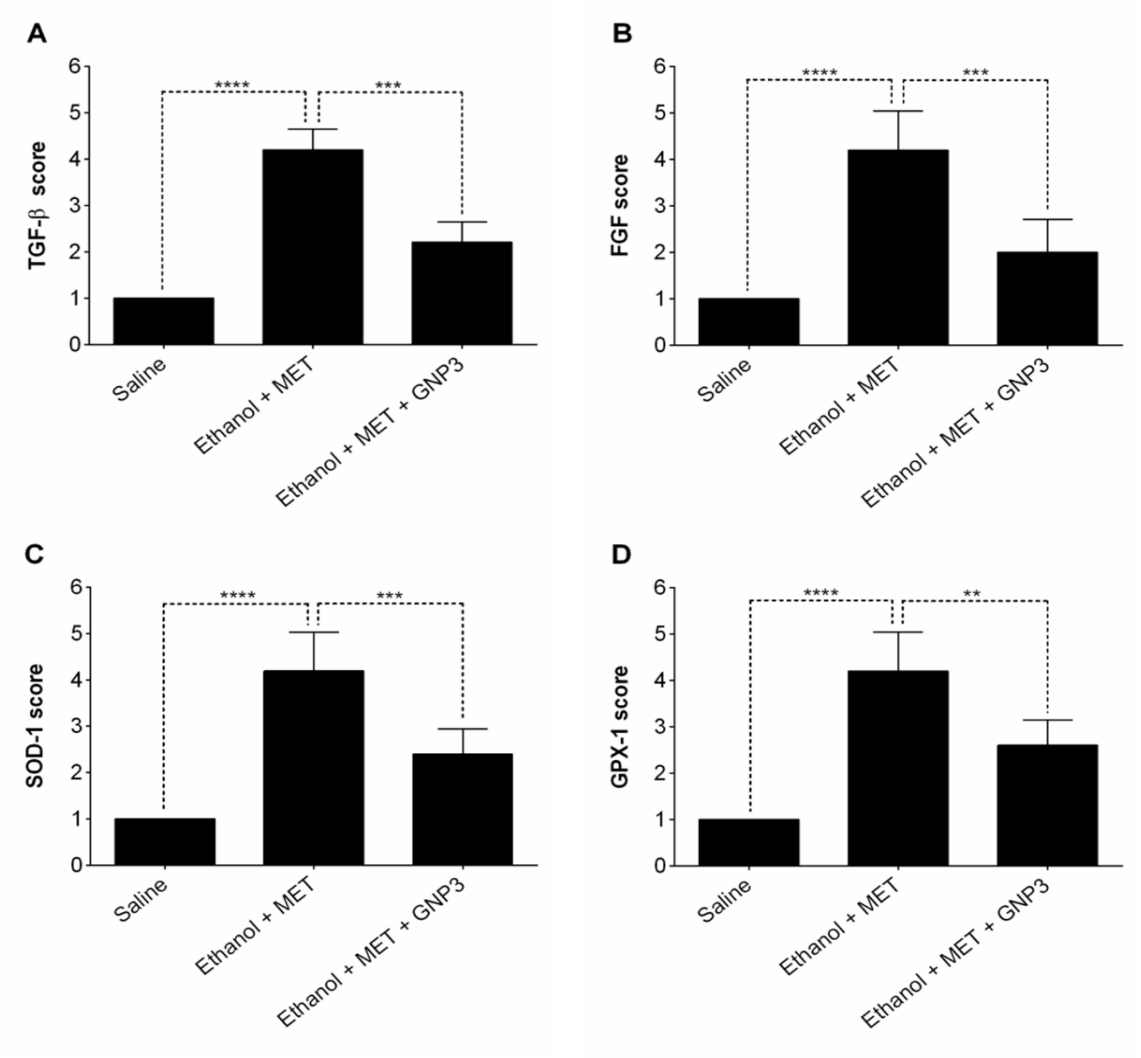

Figure 7. Immunohistochemistry scores. Graphical representation of the mean scores from alcohol + methamphetamine + GNP 724.96 µg/kg treated group for TGF-β (A), FGF (B), SOD-1 (C) and GPX-1 (D) immunoreactivity. ** $p < 0.01$; *** $p < 0.001$; **** $p < 0.0001$.

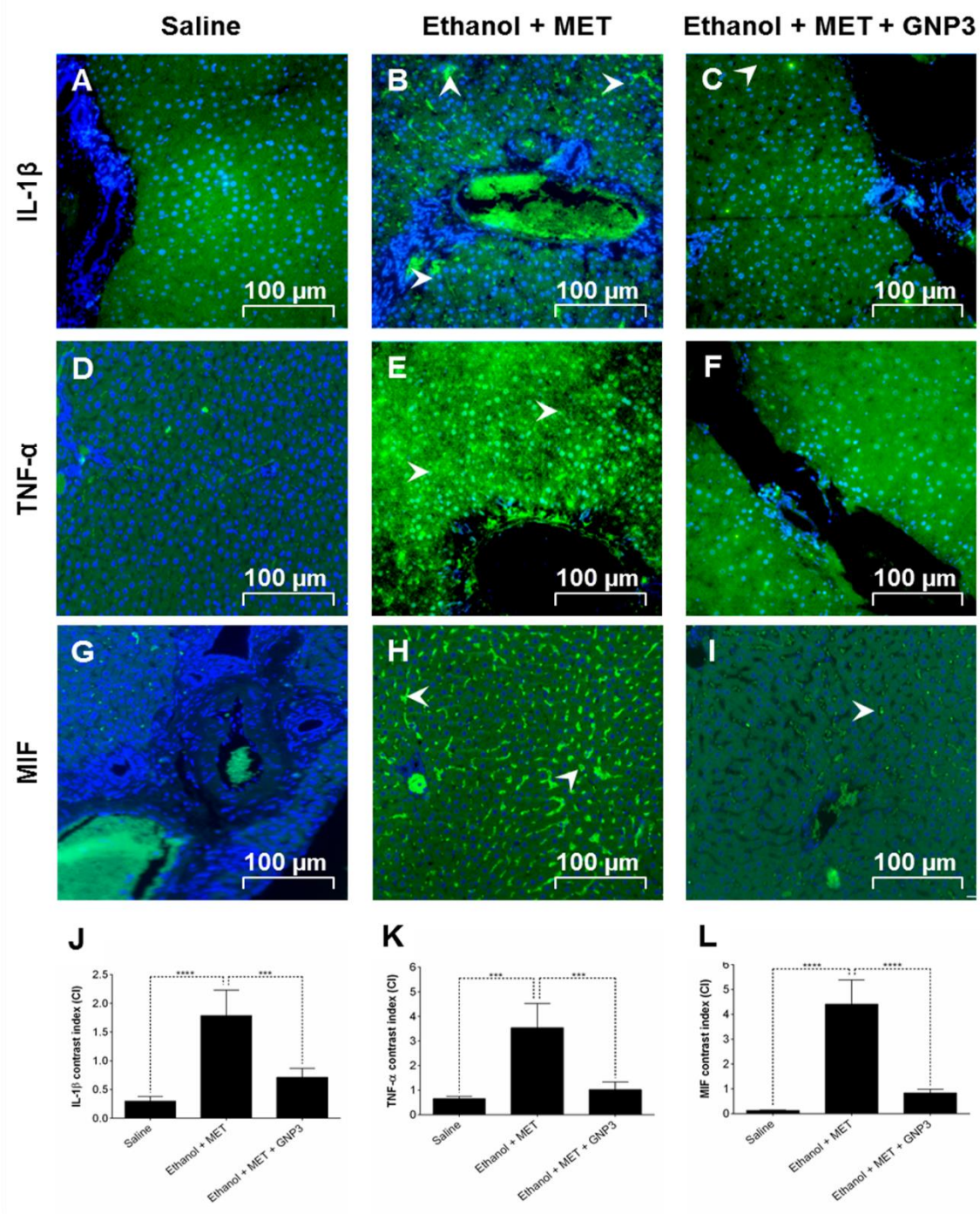

Figure 8.Modulation of expression of IL-1β, TNF-α and MIF. Representative photomicrographs of IL-1β(A-C), TNF-α(D-F) and MIF(G-I) immunoreactivity in liver specimens from each group (green) with DAPI nuclear counterstained (blue).Graphical representation of the contrast index from IL-1β (J), TNF-α (K) and MIF (L). METH, methamphetamine; GNP3, gold nanoparticles 724.96 µg/kg.***$p < 0.001$; ****$p < 0.0001$.

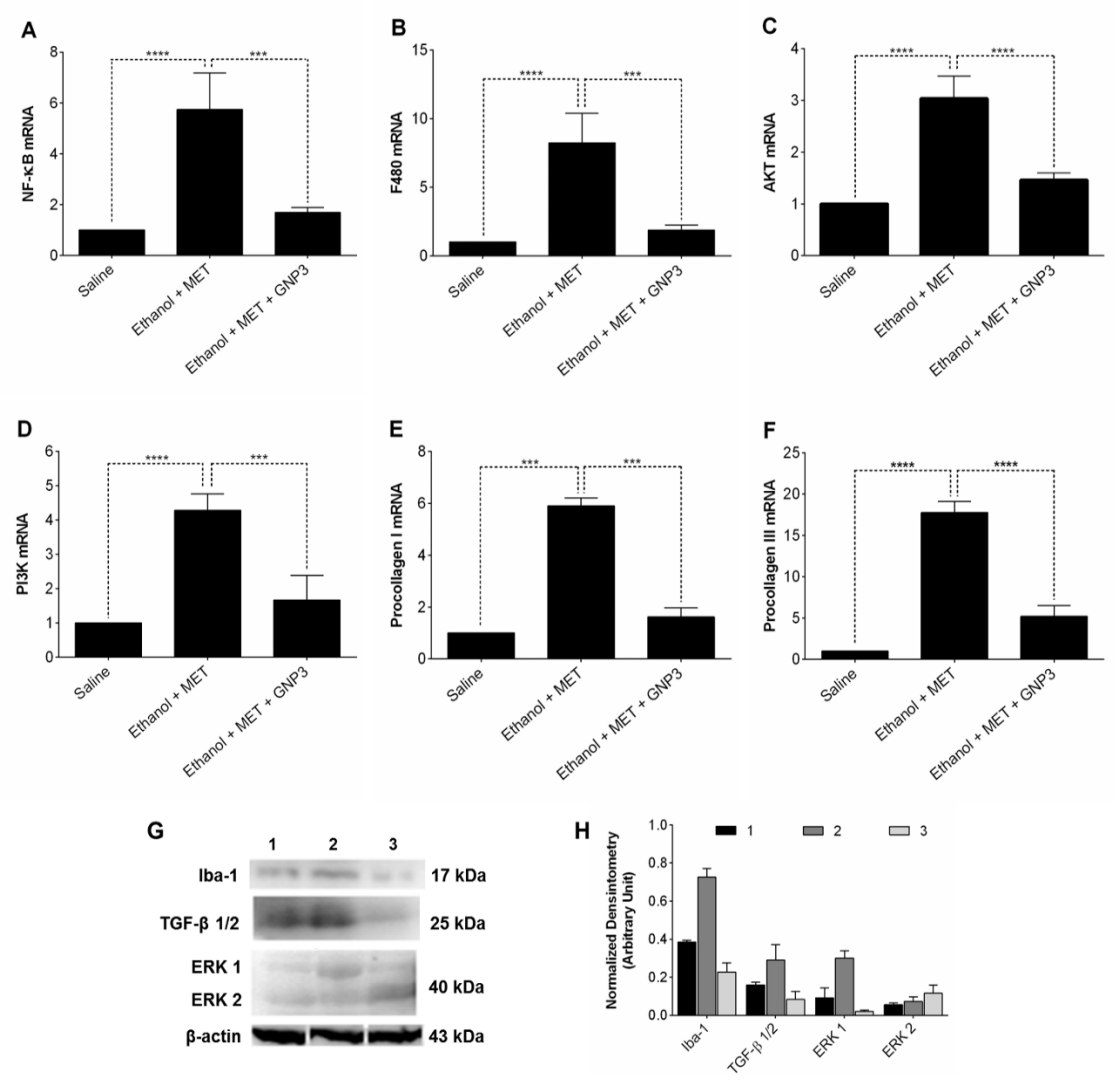

Figure 9. Gene expression at mRNA and protein levels. Relative mRNA expression from NF-κB (A), F480 (B), AKT (C), PI3K (D), Procollagen I (E) and Procollagen III (F) genes. Results are presented as fold-change of the media values, normalized to glyceraldehyde 3-phosphate dehydrogenase (GAPDH) and expressed by mean ± SEM (**$p < 0.001$; ****$p < 0.0001$). Protein expression from IBA-1, ERK1/ERK2 and TGF-β genes (Fig. 09.G) was detected in total protein extracts determined by western blot, with detection of β-actin used as a loading control. Graphical representation densitometry analysis the result of analysis western blot (Fig 09.H). METH, methamphetamine; GNP3, gold nanoparticles 724.96 µg/kg. In Figure 9G figures 1, 2 and 3 represent the analyzed groups 1-negative control group, 2-positive control group and 3 group treated with GNPs 724.96 µg/kg. Data were representative of at least two similar experiments.

mRNA	Oligonucleotide primers	Annealing primer temperature
GAPDH	forward: 5' AAC TTT GGC ATC GTG GAA GG 3' reverse: 5' GTG GAT GCA GGG ATG ATG TTC 3'	60ºC
NF-κβ	forward: 5' TCT GCT TCC AGG TGA CAG TG 3; reverse: 5' ATC TTG AGC TCG GCA GTG TT 3'	55,2ºC
PCI	forward: 5' CAG GGA GTA AGG GAC ACG AA 3'; reverse: 5' TCC CAC AGC AGT TAG GAA CC 3'	56,8ºC
PCIII	forward: 5' ATG GTG GCT TTC AGT TCA GC 3'; reverse: 5' TGG GGT TTC AGA GAG TTT GG 3'	*55,2ºC*
F4/80	forward: 5' GCC CTT CCA ACT CAT GT 3' reverse: 5' AGG GAA TCC TTT TGC ATG TG 3'	55,1ºC
AKT	forward: 5' TCA CCT CTG AGA CCG ACA CC 3' reverse: 5' ACT GGC TGA GGA GAA CTG G 3'	58,5ºC
PI3K	forward: 5' AAC TTG GCA TGG AAG G 3', reverse: GTG GAT GCA GGG ATG ATG TTC 3'	55,5ºC

Table 1. Primer Sequences used for PCR

9 – REFERÊNCIAS

1. Almeida, S. P.; Silva, M. T. A. Histórico, efeitos e mecanismo de ação do êxtase (3-4 metilenodioximetanfetamina): revisão da literatura. Revista Panamericana de Salud Pública, São Paulo, 06 mar. 2000.
2. Martins, E. R. C.; Corrêa, A. K. Lidar com substâncias psicoativas: o significado para o trabalhador de enfermagem. Revista Latino-americana de Enfermagem, Ribeirão Preto, v. 12, 15 mar. 2004.
3. Winkler MC, Greager EM, Stafford J, Bachtell RK. Methamphetamine self-administration reduces alcohol consumption and preference in alcohol-preferring P rats. Addict Biol. 2016;
4. Yan J, Abdelgawad AM, El-Naggar ME, Rojas OJ. Antibacterial activity of silver nanoparticles synthesized In-situ by solution spraying onto cellulose. Carbohydr Polym. 2016;147:500–8.
5. 3. Kedia S, Sell MA, Relyea G. Mono- versus polydrug abuse patterns among publicly funded clients. Subst Abuse Treat Prev Policy. 2007;2:33.
6. Jang GR, Harris RZ. Drug interactions involving ethanol and alcoholic beverages. Expert Opin Drug Metab Toxicol. 2007;3(5):719–31.
7. Hamida S Ben, Bach S, Plute E, Jones BC, Kelche C, Cassel JC. Ethanol-ecstasy (MDMA) interactions in rats: Preserved attenuation of hyperthermia and potentiation of hyperactivity by ethanol despite prior ethanol treatment. Pharmacol Biochem Behav. 2006;84(1):162–8.
8. Pontes H, Santos-Marques MJ, Fernandes E, Duarte JA, Remiao F, Carvalho F, et al. Effect of chronic ethanol exposure on the hepatotoxicity of ecstasy in mice: An ex vivo study. Toxicol Vitr. 2008;22(4):910–20.
9. Ikegami A, Olsen CM, Fleming SM, Guerra EE, Bittner MA, Wagner J, et al. Intravenous ethanol/cocaine self-administration initiates high intake of intravenous ethanol alone. Pharmacol Biochem Behav. 2002;72(4):787–94.
10. Zenulka O, Sabová M, Juřica J, MacHalíček M, Švéda P, Farková M,

et al. The effect of methamphetamine on biotransformation of ethanol: Pilot study. Acta Fac Pharm Univ Comenianae. 2012;59(2):63–71.

11. Lieber, C. S., (2000). Alcohol and the Liver: metabolism of alcohol and its role in hepatic and extrahepatic diseases, The Mount Sinai Journal of Medicin, 67 (1), pp. 84-94.
12. Koriem KMM, Soliman RE. Chlorogenic and caftaric acids in liver toxicity and oxidative stress induced by methamphetamine. J Toxicol. 2014;2014.
13. Pontes H, Duarte JA, de Pinho PG, Soares ME, Fernandes E, Dinis-Oliveira RJ, et al. Chronic exposure to ethanol exacerbates MDMA-induced hyperthermia and exposes liver to severe MDMA-induced toxicity in CD1 mice. Toxicology. 2008;252(1–3):64–71.
14. Guo R, Zhong L, Ren J. Overexpression of aldehyde dehydrogenase-2 attenuates chronic alcohol exposure-induced apoptosis, change in akt and pim signalling in liver. Clin Exp Pharmacol Physiol. 2009;36(5–6):463–8.
15. Yin HQ, Kim YC, Chung YS, Kim YC, Shin YK, Lee BH. Honokiol reverses alcoholic fatty liver by inhibiting the maturation of sterol regulatory element binding protein-1c and the expression of its downstream lipogenesis genes. Toxicol Appl Pharmacol. 2009;236(1):124–30.
16. Tang Y, Li Y, Yu H, Gao C, Liu L, Xing M, et al. Quercetin attenuates chronic ethanol hepatotoxicity: Implication of “free” iron uptake and release. Food Chem Toxicol. 2014;67:131–8.
17. Chen Y-L, Chen L-J, Bair M-J, Yao M-L, Peng H-C, Yang S-S, et al. Antioxidative status of patients with alcoholic liver disease in southeastern Taiwan. World J Gastroenterol. 2011;17(8):1063–70.
18. Stewart, S. F., et al. (2004). Oxidative stress as a trigger for cellular immune responses in patients with alcoholic liver disease, Hepatology, 39, pp. 197-203.
19. Gao, B. e Bataller, R. (2011). Alcoholic liver disease: pathogenesis and new therapeutic targets, Gastroenterology 141(5), pp. 1572-85.
20. Breitkopf, K., et al. (2009). Current Experimental Perspectives on the

Clinical Progression of Alcoholic Liver Disease, Alcoholism: Clinical and Experimental Research, 33, pp. 1647-1655.

21. Arteel, G. (2003). Advances in alcoholic liver disease, Best Practice & Research Clinical Gastroenterology, 17, pp. 625-647.
22. Trabut, J.B et al., 2012. Hépatite alcoolique aiguë, La Revue de Médecine Interne, 33, pp. 311-317.
23. Tsukada, S., et al. (2006). Mechanisms of liver fibrosis, Clinica Chimica Acta, 364, pp. 33-60.
24. Bataller, R. e Brenner, D. A. (2005). Liver fibrosis, The Journal of Clinical Investigation, 115, pp. 209-218.
25. Pinzani, M. e Rombouts, K. (2004). Liver fibrosis: from the bench to clinical targets. Digestive and Liver Disease, 36, pp. 231-242.
26. Park HY, Choi HD, Eom H, Choi I. Enzymatic modification enhances the protective activity of citrus flavonoids against alcohol-induced liver disease. Food Chem. 2013;139(1–4):231–40.
27. Kang NJ, Lee KM, Kim JH, Lee BK, Kwon JY, Lee KW, et al. Inhibition of gap junctional intercellular communication by the green tea polyphenol (-)-epigallocatechin gallate in normal rat liver epithelial cells. J Agric Food Chem. 2008;56(21):10422–7.
28. Son Y, Cheong Y-K, Kim N-H, Chung H-T, Kang DG, Pae H-O. Mitogen-Activated Protein Kinases and Reactive Oxygen Species: How Can ROS Activate MAPK Pathways? J Signal Transduct [Internet]. 2011;2011:792639.
29. Wen D, Huang X, Zhang M, Zhang L, Chen J, Gu Y, et al. Resveratrol attenuates diabetic nephropathy via modulating angiogenesis. PLoS One. 2013;8(12).
30. Reif S, Lang A, Lindquist JN, Yata Y, Gäbele E, Scanga A, et al. The role of focal adhesion kinase-phosphatidylinositol 3-kinase-Akt signaling in hepatic stellate cell proliferation and type I collagen expression. J Biol Chem. 2003;278(10):8083–90.
31. Bartneck M, Warzecha KT, Tacke F. Therapeutic targeting of liver inflammation and fibrosis by nanomedicine. Hepatobiliary Surg Nutr. 2014;3(6):364–76.

32. He W, Cheng ZH, Yuan FL, Jian PX, Rong GY, Pei FZ, et al. One-step label-free optical genosensing system for sequence-specific DNA related to the human immunodeficiency virus based on the measurements of light scattering signals of gold nanorods. Anal Chem. 2008;80(22):8424–30.
33. Gunes Y, Y LY, Gumrukcuoglu HA, Tuncer M. Role of echocardiography in the evaluation of atrial function and diseases. Minerva Cardioangiol. 2010;58(3):379–97.
34. Aslan K, Lakowicz JR, Geddes CD. Nanogold-plasmon-resonance-based glucose sensing. Anal Biochem. 2004;330(1):145–55.
35. Dykman LA, Bogatyrev VA. Use of the dot-immunogold assay for the rapid diagnosis of acute enteric infections. FEMS Immunol Med Microbiol. 2000;27(2):135–7.
36. Hirsch LR, Stafford RJ, Bankson JA, Sershen SR, Rivera B, Price RE, et al. Nanoshell-mediated near-infrared thermal therapy of tumors under magnetic resonance guidance. Proc Natl Acad Sci U S A. 2003;100(23):13549–54.
37. Aravinthan A, Kamala-Kannan S, Govarthanan M, Kim J-H. Accumulation of biosynthesized gold nanoparticles and its impact on various organs of Sprague Dawley rats: a systematic study. Toxicol Res [Internet]. 2016;5(6):1530–8. Available at: http://xlink.rsc.org/?DOI=C6TX00202A
38. De M, Rotello VM. Synthetic “chaperones”: nanoparticle-mediated refolding of thermally denatured proteins. Chem Commun (Camb). 2008;(30):3504–6.
39. Schaeublin NM, Braydich-Stolle LK, Schrand AM, Miller JM, Hutchison J, Schlager JJ, et al. Surface charge of gold nanoparticles mediates mechanism of toxicity. Nanoscale. 2011;3:410–20.
40. 31. Loumaigne M, Richard A, Laverdant J, Nutarelli D, Débarre A. Ligand-induced anisotropy of the two-photon luminescence of spherical gold particles in solution unraveled at the single particle level. Nano Lett. 2010;10(8):2817–24.
41. 32. Fröhlich E. The role of surface charge in cellular uptake and

cytotoxicity of medical nanoparticles. Vol. 7, International Journal of Nanomedicine. 2012. p. 5577–91.

42. 33. Tilg H, Moschen AR. Inflammatory mechanisms in the regulation of insulin resistance. Mol Med [Internet]. 2008;14(3–4):222–31.
43. MacParland SA, Tsoi KM, Ouyang B, Ma XZ, Manuel J, Fawaz A, et al. Phenotype Determines Nanoparticle Uptake by Human Macrophages from Liver and Blood. ACS Nano. 2017;11(3):2428–43.
44. Diogo Frasquilho GUERREIRO, Ana Lisa CARMO JA da S, Rita NAVARRO CG. CLUB DRUGS A New Profile of Substance Abuse in Adolescents and Young Adults [Internet]. Acta Med Port. 2011. p. 739–56.
45. Mincis M, Mincis R. Esteatose e esteato-hepatite não alcoólicas. Vol. 63, Revista Brasileira de Medicina. 2006. p. 564–70.
46. El-Naggar ME, El-Rafie MH, El-sheikh MA, El-Feky GS, Hebeish A. Synthesis, characterization, release kinetics and toxicity profile of drug-loaded starch nanoparticles. Int J Biol Macromol. 2015;81:718–29.
47. Zhang Q, Hitchins VM, Schrand AM, Hussain SM, Goering PL. Uptake of gold nanoparticles in murine macrophage cells without cytotoxicity or production of pro-inflammatory mediators. Nanotoxicology. 2011;5(3):284–95.
48. De Araújo RF, Garcia VB, De Carvalho Leitão RF, De Castro Brito GA, De Castro Miguel E, Guedes PMM, et al. Carvedilol improves inflammatory response, oxidative stress and fibrosis in the alcohol-induced liver injury in rats by regulating kuppfer cells and hepatic stellate cells. PLoS One. 2016;11(2).
49. Halpin LE, Gunning WT, Yamamoto BK. Methamphetamine causes acute hyperthermia-dependent liver damage. Pharmacol Res Perspect. 2013;1(1).
50. Gasparotto LHS, Garcia AC, Gomes JF, Tremiliosi-Filho G. Electrocatalytic performance of environmentally friendly synthesized gold nanoparticles towards the borohydride electro-oxidation reaction. J Power Sources. 2012;218:73–8.
51. de Araújo RF, de Araújo AA, Pessoa JB, Freire Neto FP, da Silva GR,

Leitão Oliveira ALCS, et al. Anti-inflammatory, analgesic and anti-tumor properties of gold nanoparticles. Pharmacol Reports. 2017;69(1):119–29.

52. Esterbauer H, Cheeseman KH. Determination of aldehydic lipid peroxidation products: Malonaldehyde and 4-hydroxynonenal. Methods Enzymol. 1990;186(C):407–21.
53. Safieh-Garabedian B, Poole S, Allchorne A, Winter J, Woolf CJ. Contribution of interleukin-1 beta to the inflammation-induced increase in nerve growth factor levels and inflammatory hyperalgesia. Br J Pharmacol. 1995;115(7):1265–75.
54. Ishak K, Baptista A, Bianchi L, Callea F, De Groote J, Gudat F, et al. Histological grading and staging of chronic hepatitis. J Hepatol. 1995;22(6):696–9.
55. Zhang J, Tang H, Zhang Y, Deng R, Shao L, Liu Y, et al. Identification of suitable reference genes for quantitative RT-PCR during 3T3-L1 adipocyte differentiation. Int J Mol Med. 2014;33(5):1209–18.

Universidade Federal do Rio Grande do Norte
COMISSÃO DE ÉTICA NO USO DE ANIMAIS - CEUA

PROTOCOLO N.º **018/2015 (5)**

Professor/Pesquisador: *RAIMUNDO FERNANDES DE ARAÚJO JÚNIOR*

Natal (RN), 04 de novembro de 2015.

Certificamos que o projeto intitulado **"Avaliação da atividade antinflamatória e citotoxicidade do carvedilol, nanoconjugados e curcumina em modelo experimental de injúria hepática alcoólica associada a metanfetamina"**, protocolo 018/2015, sob a responsabilidade de RAIMUNDO FERNANDES DE ARAÚJO JÚNIOR, que envolve a produção, manutenção e/ou utilização de animais pertencentes ao filo Chordata, subfilo Vertebrata (exceto o homem), para fins de pesquisa científica encontra-se de acordo com os preceitos da Lei n.º 11.794, de 8 de outubro de 2008, do Decreto n.º 6.899, de 15 de julho de 2009, e com as normas editadas pelo Conselho Nacional de Controle da Experimentação Animal (CONCEA), e foi aprovado, após análise das adequações, pela COMISSÃO DE ÉTICA NO USO DE ANIMAIS da Universidade Federal do Rio Grande do Norte – CEUA/UFRN, em reunião de 04 de novembro de 2015.

Vigência do Projeto	**DEZEMBRO 2018**
Número de Animais	**36**
Espécie/Linhagem	**Ratos / Wistar**
Peso/Idade	**220-250g / 60 dias**
Sexo	**Machos**
Origem	**Biotério do Depto de Biofísica e Farmacologia UFRN**

Informamos ainda que, segundo o Cap. 2, Art. 13 do Regimento, é função do professor/pesquisador responsável pelo projeto a elaboração de relatório de acompanhamento que deverá ser entregue tão logo a pesquisa for concluída.

Josy Carolina Covan Pontes
Coordenadora da CEUA

UFRN – Campus Universitário – Centro de Biociências
Av. Salgado Filho, S/N – CEP: 59072-970 – Natal/RN

Celular Institucional (Claro): 9229-6491
e-mail: ceua@reitoria.ufrn.br